NASA Technical Memorandum 86169

X-Ray Spectra of Supernova Remnants

Andrew E. Szymkowiak

FEBRUARY 1985

NASA

NASA Technical Memorandum 86169

X-Ray Spectra of Supernova Remnants

Andrew E. Szymkowiak
University of Maryland
College Park, Maryland

NASA
National Aeronautics
and Space Administration

Scientific and Technical
Information Branch

1985

This Page Intentionally Left Blank

TABLE OF CONTENTS

I. Introduction

The advent of astronomical spectroscopy provided much of the impetus for the creation of astrophysics, a bridge between physics and astronomy. The ability to study composition and temperature of remote objects allowed the transition from a field mainly concerned with observing and cataloguing objects to one concerned with constructing models of the objects and how they had attained their present states. Applying spectroscopy to the X-ray band allows this exploration to be extended to hotter objects.

In studying supernovae and their remnants, we can establish bridges between other sub-disciplines of astronomy and physics. Supernovae close the cycle between the deaths of stars and the interstellar medium that will eventually condense to form the next generation of stars. Most of the atoms in the universe heavier than helium were created in the interior of stars. Some other elements may only be created in the high neutron fluxes that occur during supernova explosions. Supernovae supply one of the means by which these elements get circulated out into the galaxies. Their shockwaves may trigger the collapse of clouds that then form stars and planets (Cameron and Truran 1977). In an earlier epoch, the combined winds from supernovae in young galaxies may have been able to sweep up huge shells of inter-galactic medium, which then fragmented into a new collection of galaxies (Ostriker 1983). In addition to their effects upon the evolving universe, as bright "standard candles" supernovae provide a good tool for the measurements over large distances required for determining the parameters of that evolution.

To model supernovae, and their effects upon the universe at large, requires details from physics at length scales ranging from the sub-atomic to the cosmological. The state of the knowledge at most of these length scales is sufficiently advanced so that there can be general agreement about what types of mechanisms are most likely to pertain to physical supernovae. Consequently, the work of the model builders is not diluted by having to explore widely different types of scenarios. On the other hand, the field is young enough so that we still can expect discoveries, rather than mere refinements to the values of the parameters of one model.

The violence of a supernova explosion is so large that the shock can heat hundreds of solar masses of material before the temperature drops below one million degrees. Thus for thousands of years, most of the material of the remnants will be emitting primarily in the X-ray. X-ray observations can directly reveal the bulk of the material, while observations in other bands usually only show a small fraction of the total remnant. X-ray spectra of the hot material are used, with models, to constrain temperatures, densities, and composition. Observational constraints on these quantities directly address major unknowns in research on supernovae and the interstellar medium. By measuring the temperatures and the densities in young remnants, we place some limits on the structure and energy of the explosions. More importantly, once we have determined the physical conditions, we can determine some elemental abundances in the supernova ejecta. The composition information we can obtain with spectrometers provides good tests for the various models of what it is that happens in a supernova. This supplies a prime motivation for our investigations. In addition to learning

about supernovae, we can expect to obtain important information about the interstellar medium (ISM). By heating a region of the ISM, the older remnants provide us with distant samples of the composition of the medium. In large remnants, we can get several such samples and learn about the homogeneity of the ISM. With these measurements we assist in the effort to determine the structure of the ISM, which is maintained by the combined actions of all the processes that can heat, stir, and cool it. Determination of the structure would constrain the rates and efficiencies of the various processes over the life of the galaxy.

In the first section, we lay out the observational and theoretical background for this work. The next section addresses specific models for the production of X-rays in supernova remnants. Next we describe the specific instrumentation and the techniques we have developed for obtaining and reducing the data. The subsequent two sections present the analysis of X-ray spectra from two of the classes of objects we have studied in detail. The first of these sections concerns the supernova remnant Puppis A, an example of a "middle-aged" remnant in which the details of the explosion are no longer important and we can study the blastwave shock moving in the inhomogeneous interstellar medium. The second analysis section examines spectra taken from two of the youngest remnants known in the galaxy. In these remnants much of the emission is arising in shocked supernova ejecta, and we can study the composition of the progenitor stars. The concluding section addresses what types of information we can expect from X-ray spectroscopy of supernova remnants in the future.

II. OBSERVATIONAL AND THEORETICAL BACKGROUND

For millenia, observers of the sky have seen objects that become bright and then fade away again. Although some of these "novae" lasted much longer than the average, the existence of a separate class of super-novae was not recognized until after the emergence of the extragalactic distance scale in the 1920s. At that time, astronomers realized that the "novae" in the spiral nebulae, which had just been identified as external galaxies at great distances, must have had peak luminosities several thousand times brighter than the galactic novae. While a classical nova is a violent event, with luminosity 10^6 times that of the sun, the perturbed system can return to nearly its pre-outburst conditions after a few decades. The energies implied by the more powerful outbursts of the supernova, however, were sufficient to completely disrupt a star.

Except for several naked eye accounts in historical records, optical observers have had to rely upon extragalactic supernovae, as there have been no supernovae visible in our galaxy since before the invention of the telescope (Background information in this and the next chapter is drawn from the reviews of Woltjer, 1972; and Trimble, 1982; 1983). Approximately 300 supernovae have been observed since the modern search was started by Zwicky in 1934. We will not delve into all of the phenomenology of the observations but only touch upon the data which indicate what might be occurring in these outbursts. The optical spectra of all types of supernovae have a few features in common. A blackbody fit to the continuum yields a temperature near 11000 K at maximum light, declining to 6000 K after a few weeks. The line systems initially show velocities of order 1.5×10^4 km/sec which decline to

5×10^3 km/sec in about a month. The optical spectra during outburst appear to divide into several classes. Though only two types are referred to today, there are observations that do not clearly belong to either of the two large classes. Type I supernovae are those whose spectra do not show strong lines of hydrogen, while Type II supernovae are those that do. The Type I form a very homogeneous class; they show little variation in absolute magnitude, spectra, or shape of lightcurve. A much larger variation is seen among Type II supernovae, including a few with light curves resembling those of Type I. The significant features of the Type I light curve are a smooth broad peak with a rapid rise and decline, and a long exponential decline with a half-life of approximately 50 days. Type II supernovae seem restricted to galaxies with strong spiral structure. The rate for both types increases with the fraction of massive stars in the galaxy. The conventional wisdom is that Type I supernovae arise in Population II objects, and vice versa, although the evidence is equivocal.

While the bright optical outbursts diminish after several hundred days, the supernovae can create radio sources, both compact objects and extended nebulae, that remain bright for thousands of years. Due to these long lifetimes, there is a large sample of such radio remnants available for study within the galaxy. Since the supernova of 1054 AD is known to have produced a pulsar, some supernovae must be capable of leaving a compact stellar remnant in addition to any extended remnant. A few other of the ~300 pulsars knowns are associated with supernova remnants. Most pulsars are observed to have a large velocity, as though given a kick in an explosion or slung out of a binary when the companion was disrupted. Because of these large velocities, the large galactic

scale height of the pulsars is not thought to correspond to the scale height of the progenitors; it is quite likely that they were all born in the disk population and have since traveled far off the plane. Their velocities may also serve to remove them from the remnant where they were formed. There have been difficulties in reconciling the pulsar birthrate with the supernova rate. Although the two rates now appear to be approximately equal, recent imaging X-ray observations fail to reveal hot neutron stars within several of the young remnants (Helfand 1983). Thus while some supernovae do make neutron stars, perhaps some other mechanism is required to make the remainder "quietly".

Radio sources created by supernovae include, in addition to the compact sources, many extended remnants. Most remnants show a partial or complete circular shell. Some show a filled region of emission, which may occur in combination with a hollow shell. It is believed that these filled regions may contain a central pulsar, which is continuously supplying relativistic particles to produce the emission. Although the X-ray spectroscopy and imaging of these remnants has proved rewarding (Becker and Szymkowiak 1981; Becker, Helfand, and Szymkowiak 1982; Becker, Helfand, and Szymkowiak 1983) they will not be addressed in this work.

The "shell-like" radio remnants tend to be distributed at low heights relative to the galactic plane. This probably indicates more about the distribution of mass and magnetic fields in the galaxy than about the progenitors of supernovae, since the existence of a radio remnant requires that particles and fields be swept up from the surrounding ISM and compressed. The distances to these remnants are, for the most part,

quite uncertain. This complicates efforts to compile statistics on their size distribution, or to deduce the velocities of expansion. Estimates of these are necessary to calculate a lifetime of the average remnant, in order to deduce a remnant production rate from the number observed. These rates are, in general, approximately equal to the supernova rate in gas rich galaxies but lower in the gas poor ones. This offers additional evidence that a supernova in a region of low ISM density may not leave a (long-lived) remnant.

Early surveys indicated that the size and brightness distributions of radio remnants were consistent with expansion in a uniform density medium. Recent larger samples in our galaxy and relatively complete samples from nearby galaxies, made possible by the new generation of radio interferometers, have placed this simple model in question (Mills 1983). Deviations from the simple expansion law could be due to a distribution in explosion energies, to a distribution in interstellar densities, or to an evolution modified by energy being used to evaporate clouds or compress magnetic fields.

Models for the Explosions

There are several paths that a star may take to evolve into a supernova. Just six years after Chadwick's discovery of the neutron, Zwicky (1938) suggested that collapse to a neutron star would release about 10^{51} ergs. No details were provided as to how the energy gets out and creates a supernova. There are several current scenarios for the collapse of the core of a star, to either a neutron star or black hole. A star in the 15-100 solar mass range will evolve relatively

quickly to the point where, in the central regions, the silicon burning shell creates a central core of iron group elements. As the nuclear binding energy is at a maximum in the iron group, no further burning is possible and the mass of the core continues to increase. As the mass approaches 1.5 solar masses, the central temperature rises above 3×10^9 K, and photodisintegration of the nuclei begins. This reduces the pressure in the core and the center begins collapsing. In lighter, 8 to 12 solar mass stars, a similar collapse begins when degenerate electrons in the oxygen core start being captured on ^{20}Ne and ^{24}Mg before oxygen burning can commence.

The light curves and spectra of Type II events can be produced by any mechanism that releases more than 10^{51} ergs at the base of an extended envelope of solar composition material. Although the preceding two models appear to meet this apparently modest condition, it has proved difficult to couple the energy to the material in such a way as to eject some of it. The energy of the collapse could provide outgoing momentum to the envelope material from a shock reflected from the core material by a sudden stiffening of the equation of state as it is compressed beyond nuclear densities and/or from coupling to the flux of neutrinos from the core. Both mechanisms depend upon uncertain cross sections of high energy physics and details are still changing as that physics is re-calculated. Although much effort has been expended to demonstrate the commonly held conviction that a Type II supernova can result from core collapse and bounce, no model has been able to convincingly eject a large amount of envelope (Hillebrandt 1982). Usually the reflected shock from the core dies out and the outer layers, although initially moving outward, do not attain escape velocity and fall back in.

The hope for these models is that ejection may be possible if the star were rapidly rotating. The few initial attempts at rotating models have produced ejection of an equatorial ring (Bodenheimer and Woosley 1983). There is observational evidence for expanding rings in several remnants (Lasker 1978; Tuohy, Clark, and Burton 1982; Markert et al. 1983).

The early-time optical lightcurves and spectra of Type I supernovae can be duplicated by models that deposit 10^{51} ergs into a compact star that is missing its hydrogen envelope. The slow decline in the light curves seen at late times presents more of a puzzle. Several models have been advanced to explain how, at these late times, some energy is being slowly released into the expanding remnant. With the proper configuration of an extended envelope, the energy could escape at the appropriate rate due to diffusion. A pulsar, or other compact object, could store some energy in rotation which is pumped out, perhaps as fields and particles, over an extended period. Currently in vogue are models in which the late time luminosity is powered by radioactive decay of isotopes produced by the large neutron fluxes that occur during the explosion. The luminosity and lightcurve are well fit by models with 0.25-1.4 solar masses of ^{56}Ni, which decays to ^{56}Co with a 6 day half life, and then to ^{56}Fe with a 77 day half life. Such quantities of radioactive nickel could be produced by explosions in several types of stars. Stars in the range 1.4-4 solar masses, which have somehow become well mixed during early evolution, could evolve into systems which resemble the helium cores formed in more massive stars. These cores, which can form in 4 to 10 solar mass stars on the main sequence, can explode when carbon or oxygen ignites. Because the carbon and/or oxygen

burning takes place at high temperatures, the elements can go into nuclear statistical equilibrium, and large amounts of iron peak elements can be formed. In some of the scenarios (carbon detonation) the burning begins in the center and could completely disrupt the star; while in others (involving off-center ignition, carbon deflagration or convective overturn) the burning is partially quenched and some of the star may collapse into some type of compact remnant rather than being ejected. Such models, in which all the iron that is created is not dispersed into the ISM, may alleviate the over-enrichment of the galaxy in metals which would occur if all Type I supernovae ejected such large quantities of iron (Tinsley 1979).

In addition to the above models for the creation of Type I supernovae from single stars, are those in which mass transfer in a binary system modifies the evolution of one star and causes it to explode. In these models, the initially more massive star expands, transfers its outer envelope onto the companion, and becomes a white dwarf. Later, the second star expands and starts transfering mass onto the dwarf. In some range of mass transfer rates, the dwarf can be pushed over the Chandrasekhar limit without having previously burned the accreted material. At this point the dwarf resembles the degenerate core that can form in massive stars, and can undergo similar explosions. As a large percentage of stars occur in binaries, only a small fraction need to become supernovae to match the Type I rates. The large velocities of many pulsars and the existence of pulsars in binary systems can be explained by these scenarios.

The Local Environment

These supernova explosions will affect the structure of the ISM, and the expansion of the remnants will, in turn, depend upon that structure. Locally, the environment will depend upon the pre-supernova evolution of the progenitor. Beyond this region, conditions will depend on the history of the other stars in the immediate association or cluster. There are several types of modifications possible. Large stellar winds, such as those of massive O stars, tend to evacuate a region around the star to subnormal density. Such a period of mass loss is required in some of the models for Type Is to remove the hydrogen envelope. The combined winds from the many stars of an OB association may create a low density superbubble. In the immediate vicinity of the star, a constant wind can establish a r^{-2} density distribution. The supernova shock will be accelerated as it travels down this gradient. Some of the stars missing their outer envelopes may have lost them in a more abrupt fashion. In several of the models the envelope is lost in a nova-like thermonuclear flash, leaving a planetary nebula which the later supernova shock encounters. The quasi-stationary flocculi in Cas A and similar optical patches in the Kepler remnant are believed to be pieces of ejected envelope now being shocked by the supernova blast wave. In addition to the environmental modifications caused by normal stellar evolution, supernova remnants are going to encounter cavities left by previous supernovae. This is particularly probable in OB associations where the conglomeration of young, rapidly evolving stars is apt to have supernovae relatively frequently. The bubbles around the associations may be inflated by both stellar winds and supernovae. In the galactic

disk, away from hot bubbles, a remnant would expand until it broke through into the network of tunnels left behind by past supernovae (Smith 1977). At this point the pressure in the remnant rushes into the old network, perhaps weakly re-shocking the nearby tunnel walls. This would modify statistics of remnant sizes as none will expand to diameters larger than the distance between tunnels. The existence of such tunnels may explain the peculiar morphologies of some remnants, which are often not the perfect spheres predicted for a homogeneous medium, but show straight sections and apparent "blowouts". These bubbles and tunnels, filled with hot, low density material, will rise buoyantly away from the galactic plane. As they break out of the top of the disk their material may continue to rise and may produce a "galactic fountain" which is one model for how the hot halo material, which has been detected via its absorption lines, is produced and maintained so distant from the galaxy.

In addition to heating some of the ISM, the supernovae work to redistribute it. The remnants sweep the ISM into shells which then can cool radiatively and collapse into clouds. The steady state action of supernovae is invoked to maintain the phases of a multi-state model of the ISM (McKee and Ostriker 1977). In turn, the density inhomogeneities of the multi-phase ISM affect the evolution of a supernova remnant as it must do work to evaporate clouds which it encounters (Cowie, McKee, and Ostriker 1981). Supernovae also must serve to tangle up, and perhaps amplify by creating turbulence, the galactic magnetic field. They are believed to be responsible for much of the cosmic ray acceleration in the galaxy. It is difficult to accurately estimate how the work done on the magnetic fields and cosmic rays will affect the remnant evolution.

The magnetic and cosmic ray pressures are much smaller than that behind the shock wave until quite near the end of the remnant's evolution, and are neglected in the analysis here.

III. THEORY FOR THE X-RAY EMISSION

The preceding section presented the aspects of observations and theories of the supernova outbursts relevant to the analysis of the X-ray results. In this section the specific theory of X-ray emission in remnants that are not affected by pulsars is examined. Conventionally, the life of a supernova remnant is divided into four phases (Shklovsky 1968; Woltjer 1970; Woltjer 1972). In the first, typically lasting a few hundred years, the material of the disrupted star expands ballistically. As the stellar ejecta encounters and sweeps up the circumstellar material, it begins to decelerate. After it has swept up a few times its original mass, the specific details of the explosion are no longer important, and the remnant enters the second phase. It continues in this adiabatic expansion phase for as long as radiative losses are negligible and the energy is approximately conserved. After the shock velocity has declined to about 200 km/sec the radiative cooling time of the post shock material becomes short and it forms a cool, dense shell. This shell then expands with constant radial momentum. In the fourth phase, the pressure in the remnant has dropped to the interstellar value and the remnant loses its identity as such, although the region that was the interior may remain warmer than the surroundings. This four phase picture is for an isolated remnant in a homogeneous ISM and must be modified if the remnant expands into a molecular cloud or into the cavity of another supernova remnant.

Most of the models that we will consider are those of the second phase. The typical remnant spends on the order of several times 10^4 years in this phase. This phase of adiabatic expansion is often called

the Sedov or Sedov-Taylor phase after the theorists who first developed the formulae for the expansion of a shock wave from a point explosion in an initially cold, homogeneous medium (Sedov 1959; Taylor 1950). Shklovsky (1962) initially suggested applying the Sedov solution, which had been developed for the shocks of atmospheric weapon tests, to those of supernovae. Heiles (1964) predicted that radiation from the collisional excitation of the non-hydrogenic atoms in the remnant could dominate the cooling and that the hot material in the SNR shells would be a bright source of X-rays. The expansion during this phase is self-similar; the functional forms of the physical quantities in the interior of the blastwave retain the same shape during this time. The rate of expansion, and the values of the quantities at the periphery are given by simple formulae which can be obtained by dimensional analysis (Sedov 1959). For an explosion of energy E_{51} (in units of the canonical value of 10^{51} ergs) in a cold, homogeneous medium of number density n_0 (per cm^3), with adiabatic index $\gamma=5/3$, the radial position of the shock at time t_3 (age in thousands of years) is given by:

$$r = 4.97 \text{ pc } (E_{51}/n_0)^{1/5} t_3^{2/5},$$

and the post-shock temperature by:

$$T = 4.54 \text{ keV } (E_{51}/n_0)^{2/5} t_3^{-6/5}.$$

The hydrodynamics is completely determined by just two quantities; the ratio E/n_0 of the explosion energy to the density of the medium, and the age. The shock is decelerated by having to entrain the surrounding

medium, so the post-shock temperature declines with age. The interior is filled with tenuous material at high temperature since it was shocked early when the blastwave had a high shock velocity. The functional forms for some interior variables is shown in figure III.1. The

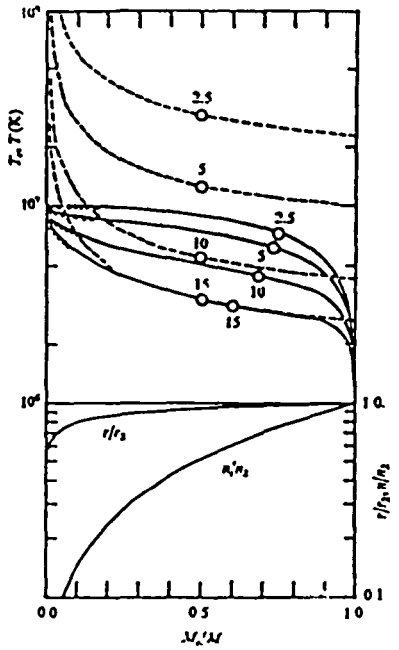

Electron temperature T_e (solid line), mean temperature T (dashed line), hydrogen density relative to the postshock value (n/n_2), and radial distance relative to the shock radius (r/r_2) as functions of the fractional mass (M_r/M) contained inside the radial distance r. Approximate analytic solutions to equation (2) obtained in Paper II are also shown (dotted line) The curves for T_e and T are for SNRs with the initial blast energy of 4×10^{50} erg and the ambient interstellar density of 0.2 H cm^{-3} and are labelled by the time elapsed since the supernova explosion in units of 10^3 yr. The open circles denote the electron temperatures $\langle T_e \rangle$ or the mean temperatures $\langle T \rangle$ which are spatially averaged over the remnant weighted by the square of the hydrogen density n^2.

FROM ITOH (1979a)

Figure III.1: The values of temperature (solid) and density (dashed) relative to their values at the shock, versus radius.

surrounding material is compressed to four times the ambient density, the appropriate value for any strong shock in a γ=5/3 gas. Most of the remnant material is concentrated into a thin shell; 20% of the mass is found outside 98% of the radius. The distribution of density gives a factor of 2.07 more emission measure (n^2V) than the preshock density over the volume of the remnant. For the Sedov solution, the emission-

weighted average temperature is 1.29 times larger than the current shock temperature. This assumes that thermal conduction is negligible in the radial direction. In an older remnant the magnetic fields will tend to be tangential which will suppress any radial conduction. If the other extreme, perfect conduction, is assumed, isothermal blastwave models (Solinger, Rappaport, and Buff 1975) would apply, although the emission predicted using these models is quite similar to that of the Sedov models.

Various levels of sophistication are possible in modelling the X-ray emission from a remnant. In the simplest model, the remnant is approximated by a series of shells, each with density and temperature given by the Sedov equations. The radiation from each shell is determined using models of an optically thin, equilibrium plasma.

The details of the line radiation produced in a hot plasma depends upon the population of the ionic states. Due to the exceedingly small densities, these cannot be calculated simply from the Boltzmann factors. The population of each state is determined by the relative rates into and out of the states, as in the standard case, but many of these transitions only function in one direction. The infrequent collisions with electrons provide the only mechanism for exciting and ionizing the atoms. An electron can produce an X-ray by collisional excitation or radiative recombination, but the reverse processes virtually never occur as the system is optically thin to those X-ray photons. Computer codes are used to calculate the ionization balance and resultant spectrum for this low density case, often called coronal equilibrium as it was first derived for the outer reaches of the sun (Cox and Tucker 1969; Mewe

1972, Raymond and Smith 1977). Many of the cross-sections, branching ratios, and rate coefficients used in these computer programs are poorly known, and specific details of the model spectra must always be viewed with caution. It is these uncertainties, combined with the uncertainties in the cosmic abundances, that usually account for the differences between models produced by different groups. We examine results from all models available to us so that the spread in results can be used as an indication of the range that can be covered by the uncertain atomic data.

Figure III.2 shows the predicted ionization states for a plasma in coronal equilibrium versus temperature, and some predicted line equivalent widths as calculated by Raymond and Smith (1977, with improvements listed in Raymond 1978, and Pravdo and Smith 1979). In the SSS data from supernova remnants, the lines from the two-electron states of Mg, Si, and S are strong, and Figure III.3 presents some ratio diagnostics for these lines for equilibrium plasmas.

The first order model for X-ray emission from supernova remnants (see Gorenstein, Harnden, and Tucker 1974, for a summary and first applications to spectral observations) assumes that the ionization instantly attains the values predicted for coronal equilibrium. In reality, heating the electrons and ionizing the atoms may require timescales that are a large fraction of the life of a remnant. At the shock, the particles are given a boost in velocity, so that the electron temperature is lower than the ion temperature by the ratio of their masses. If the only mechanism for subsequent heating of the electrons is Coulomb scattering with the hot ions, the time for equilibration

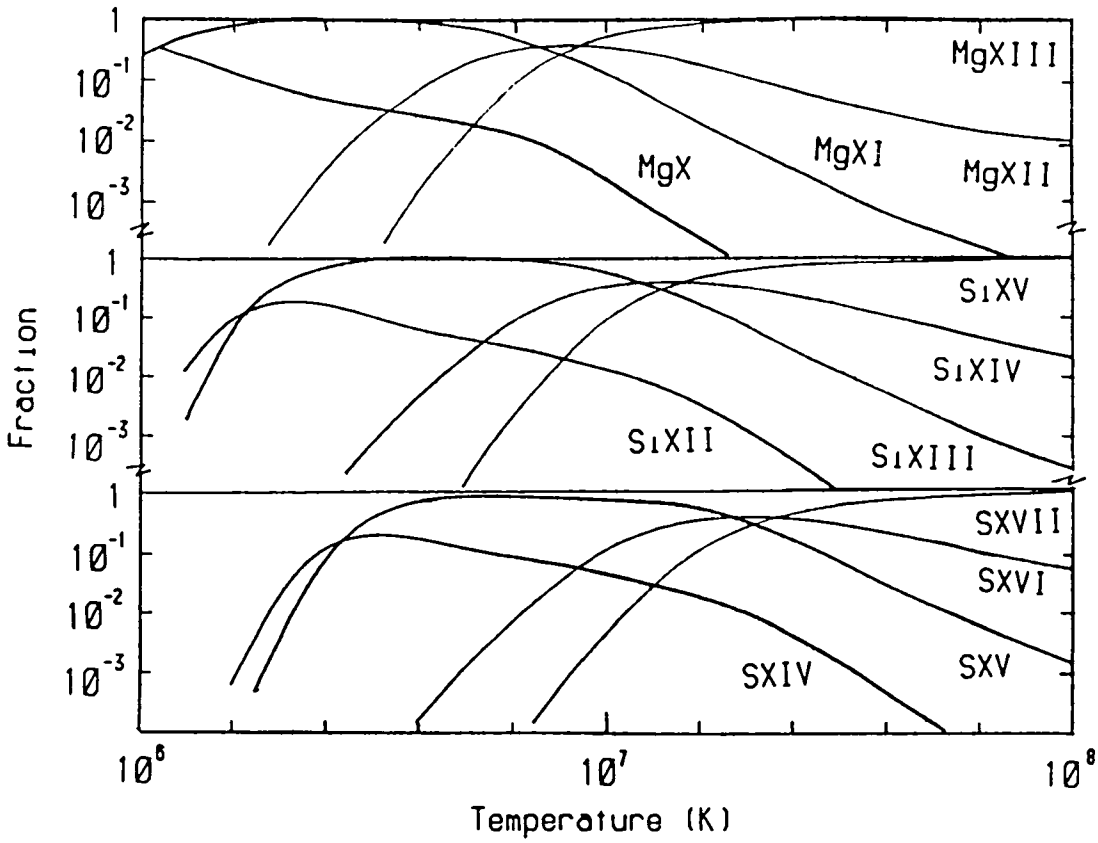

Figure III.2: Population of ionization states versus log T (K) from models of equilibrium plasma.

would be $t_{eq} \sim 2T^{3/2} n_0^{-1}$ (t in seconds, T in degrees Kelvin, n_0 number per cm^3: Spitzer 1962, 1978), or ~8000 years to bring electrons at 10^7 K to equilibrium with hotter protons at a density of 1 cm^{-3}. In this case, the X-ray continuum, determined by the slowly increasing electron temperature, would indicate a temperature much lower than that corresponding to the true shock velocity.

There are, however, several reasons to believe that the electrons equilibrate near the shock. Plasma theorists predict that microturbulence due to instabilities in the plasma will cause a fast

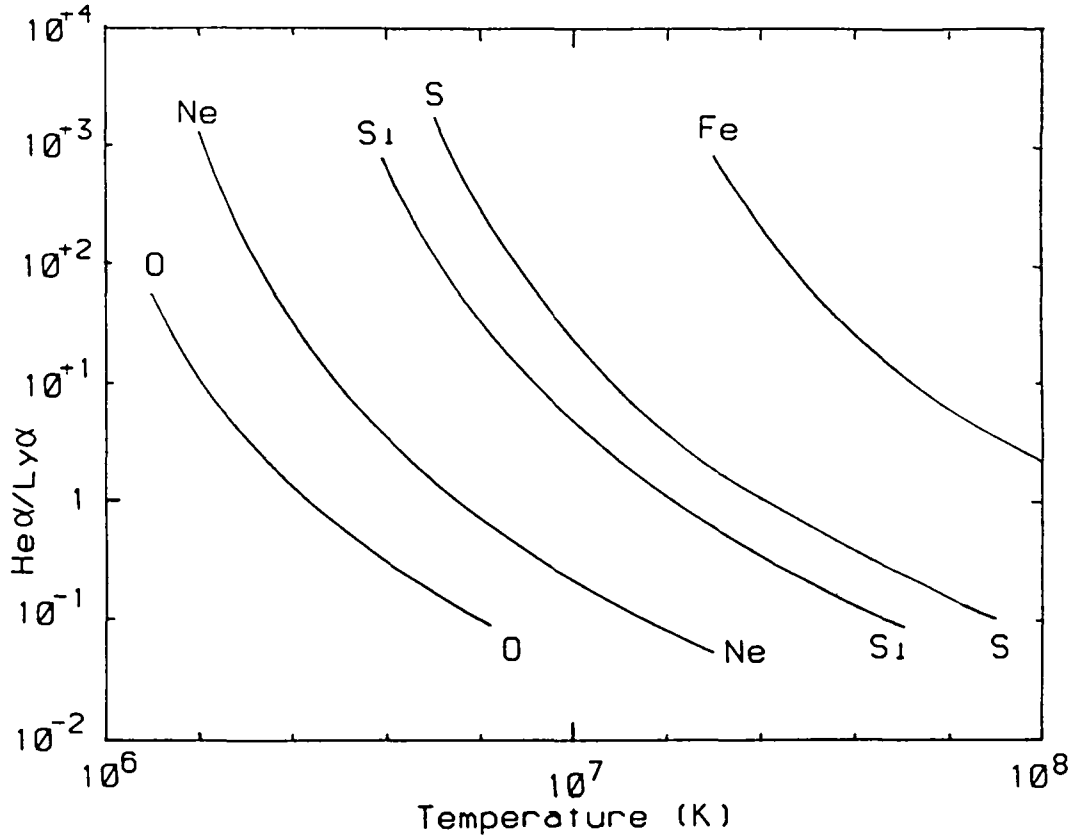

Figure III.3: Heα/Lyα line strength ratios vs T for Mg, Si, and S.

exchange of energy between the ions and the electrons (Tidman and Krall 1971; Shklovsky 1968; McKee 1970). Experimental evidence from measurements near the bow shock formed by the solar wind streaming against the Earth's magnetosphere indicates that electrons are being heated faster than by Coulomb scattering alone (see Tsurutani and Rodriguez 1981, and following papers in same volume). The bow shock electrons never completely equilibrate with the ions but remain somewhat cooler. Even if the SNR shock were more efficient than the bow shock at heating the electrons, there would be some cool electrons present from ionization of high-Z atoms in the interior. In a shock in highly enriched material, there could be sufficiently large numbers of these

cool electrons to modify the spectrum. Thus it is likely that reality lies between the extremes of slow Coulomb heating and immediate complete equilibration. In general, one should fit with models calculated for both extremes, realizing that actual remnants will occupy some middle ground.

In addition to the thermalization of the post shock electrons, various non-thermal acceleration processes in the shock may produce fast electrons. Fermi acceleration, where the electrons gain energy by being scattered back and forth across the shock, is one of the most promising mechanisms and has been investigated in the most depth. Reynolds and Chevalier (1981) consider scattering of electrons off magnetic field irregularities and show that under reasonable (but uncertain) assumptions, portions of the X-ray spectra of SNRs may be dominated by synchrotron radiation from the accelerated electrons. Such a non-thermal process may explain some unusual spectra, like the apparent power law of SN1006 (Becker et al. 1980) and the high energy tails of Cas A and Tycho (Pravdo and Smith 1979). In remnants that show conventional thermal lines, a synchrotron component from stochastically accelerated electrons may produce a high energy tail on the X-ray spectrum, so that such a tail does not necessarily indicate quick electron thermalization. More high quality, high energy X-ray observations are needed, particularly with the electron temperature diagnostics that examination of the Kα lines of Fe could provide, in order to determine the energetic electron populations.

Perhaps more significant than the simple models' neglect of the finite timescales for heating the electrons is the neglect of the length

of time required for ionization. The first order models assume that the atoms are instantly ionized to the ionic state corresponding to coronal equilibrium at the shock temperature. In reality, the collisions responsible for the ionization are so infrequent that the gas will take a long time to reach the equilibrium ionization. Figure III.4 shows a more realistic time history for the ionization following the passage of

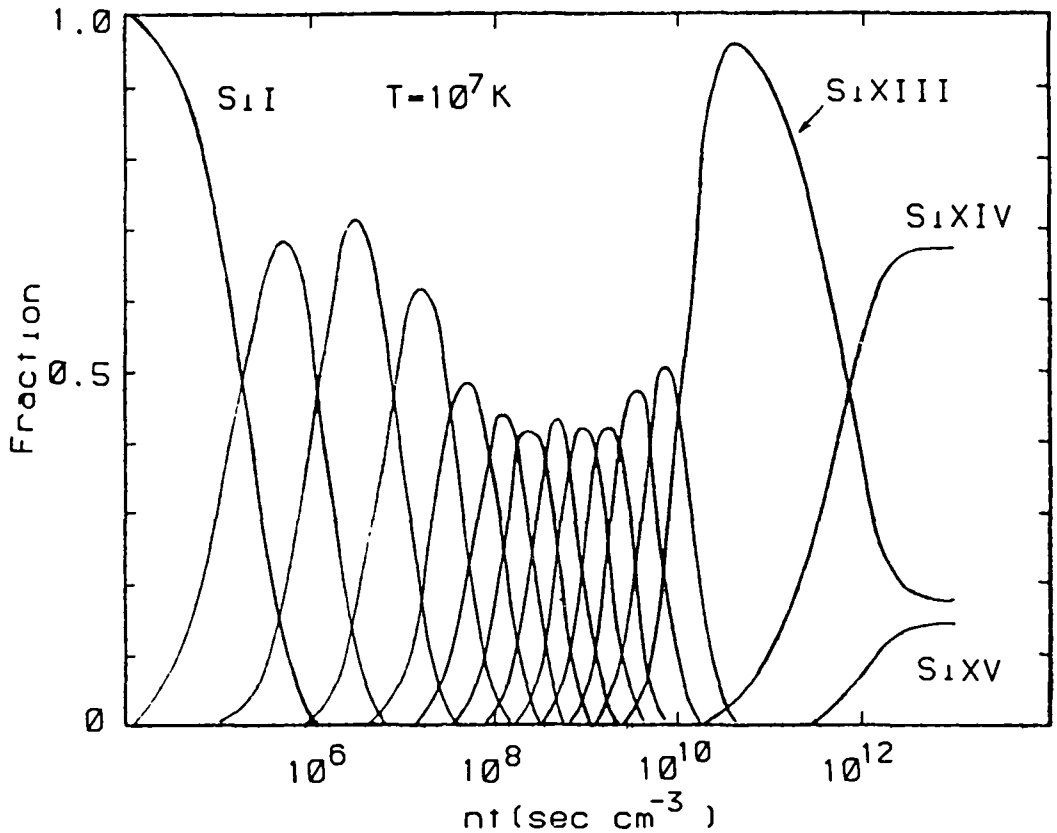

Figure III.4: The ionization fraction versus time after heating for silicon. $T=2\times10^7$ K.

a shock. The population of the ion state missing n electrons, indicated as X^{+n}, is given by:

$$\frac{dX^{+i}}{dt} = n\,[\,c^{+i-1}X^{+i-1} + \alpha^{+i+1}X^{+i+1} - X^{+i}\,(\,c^{+i} + \alpha^{+i})]$$

where α is the rate coefficient for recombination to the state (both direct and di-electronic) and c the rate coefficient for collisional ionization from the state. The figure shows the result for solving the set of coupled differential equations for a silicon atom, initially neutral, which is suddenly heated to 2×10^7 K. The ionization potentials used for calculating the collisional ionization rates were taken from Lotz (1967); the dielectronic recombination rates from Aldrovandi and Pequignot (1973). The ionization rates do not include the decrease in cross-sections at high temperatures, and so these calculations provide lower limits to the times that various ion stages begin to form. Since the ionization, excitation, and recombination rates all depend linearly upon density, the approach to equilibrium is proportional to nt, the product of the density and the age. Equilibrium is attained only after ~10000 years. Before then, the plasma will emit lines from the lower ion stages, and temperatures inferred from line measurements will be lower than the true value. While still undergoing ionization, each ion stage is present for a length of time corresponding to the amount of energy required to remove the next electron. Figure III.5 shows the ionization potentials for the innermost electrons of several elements

that have lines that fall within the range of our instrument. The energies cluster into groups corresponding to the filled electron shells. The largest gap occurs after all but the last two electrons have been removed, since the 1s shell is very tightly bound. During time-dependent ionization to states above this level, the atoms will remain in the two-electron state for a long time, so that the spectrum will tend to show lines from the transitions analogous to those that occur in the helium atom. The lowest lying and predominant transition would be the closely spaced lines of the $1s^2$-1s2p triplet, which we will refer to as the Heα line. This transition, from magnesium, silicon,

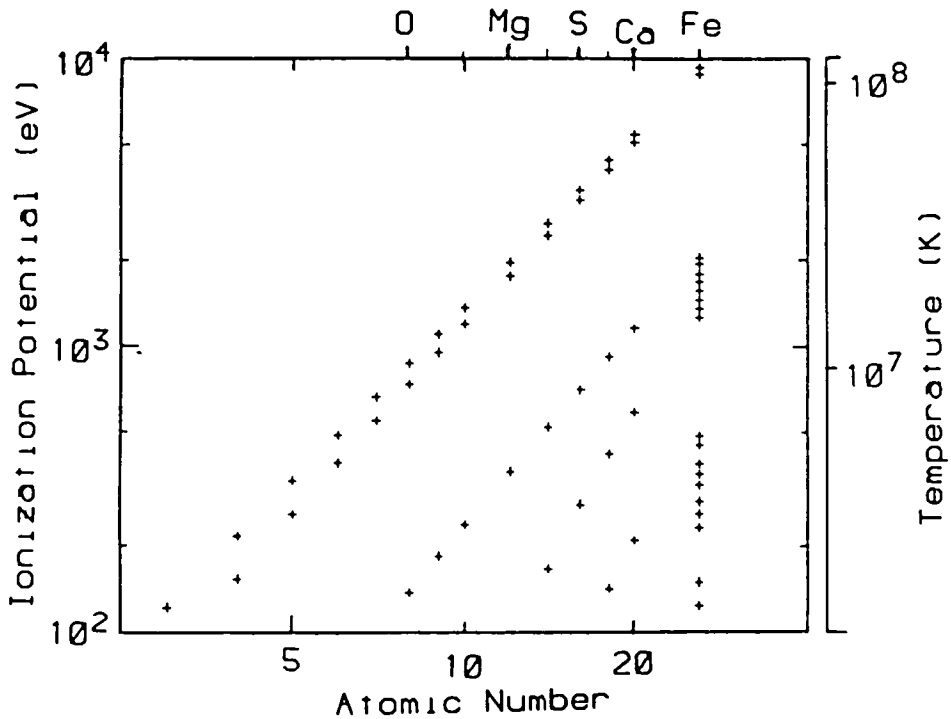

Figure III.5: Ionization potentials for some elements.

and/or sulfur is present in most of our spectra of thermal remnants, as

would be expected if few remnants have densities sufficient for fast ionization-temperature equilibration. Figure III.6, taken from Hamilton, Sarazin, and Chevalier (1983; hereafter HSC) shows the amount of enhancement of the Heα lines in Sedov remnants in the T_{shock}, η parameter plane (these parameters are defined below).

The non-equilibrium ionization will have another effect upon the

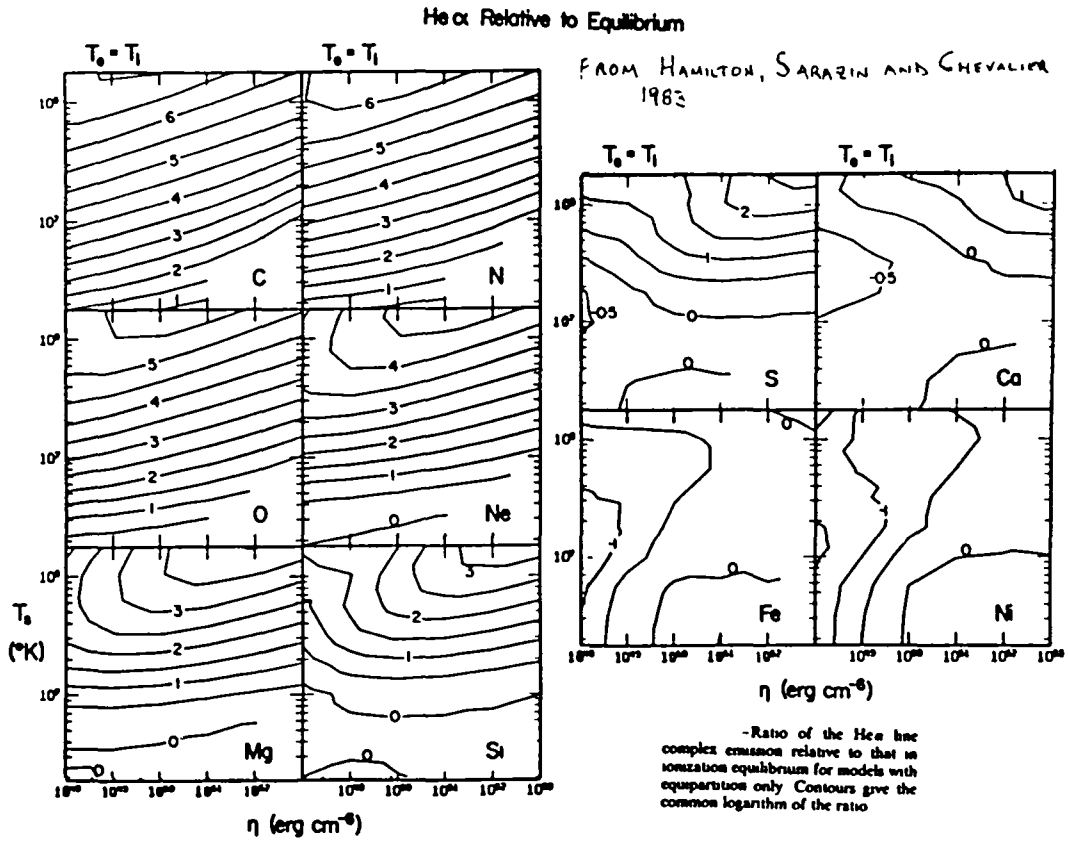

Figure III.6: The T_{shock} versus η parameter plane with contours labeled with the base 10 log of the enhancement of the silicon Heα line strength taken from Hamilton, Sarazin, and Chevalier (1983).

X-ray spectra. In addition to populating the states from which line radiation is allowed, collisional excitation will also populate metastable states. If not de-populated by collisions, these states,

forbidden by quantum selection rules from simple decay, can relax only by other processes, usually two-photon emission. In this process, the energy of the transition is divided between two photons, which carry off opposite amounts of angular momentum and permit the excited state to relax into a lower state with the same angular momentum. In ensemble, this produces a continuum bump, which is symmetric around one half the transition energy. Two photon decay from the 1s2s state to the $1s^2$ state is greatly enhanced in remnants since the ions spend so much time in the two electron ion stage.

Together the enhancements of line radiation and two-photon emission increase the amount of soft X-rays produced relative to the flux predicted for an equilibrium remnant. Figure III.7, taken from Gronenschild and Mewe (1982), compares the spectra with and without the inclusion of time-dependent ionization. Both the enhanced line emission and the two photon continuum are readily apparent. The form of the low energy enhancements can mimic that of a low-temperature equilibrium component, so that the spectrum of a non-equilibrium remnant will show this soft component rising above a continuum from a higher temperature. Figure III.8, taken from Itoh (1979), shows an example of how well the non-equilibrium spectra can be approximated by the sum of two equilibrium components. Because of this resemblance, obtaining an acceptable fit with a one or two temperature equilibrium model over a limited bandpass cannot be used as an indication that the remnant has attained equilibrium, or that two components are present. The fit temperatures for the "cool" component do not change much over the life of the remnant, so that equilibrium temperatures measured over limited band passes cannot reveal much about the age of the remnant.

Several groups have calculated spectra from non-equilibrium supernova remnants. Itoh (1977, 1978, 1979a) performed much of the initial work on the calculation of various time-dependent effects on the X-ray

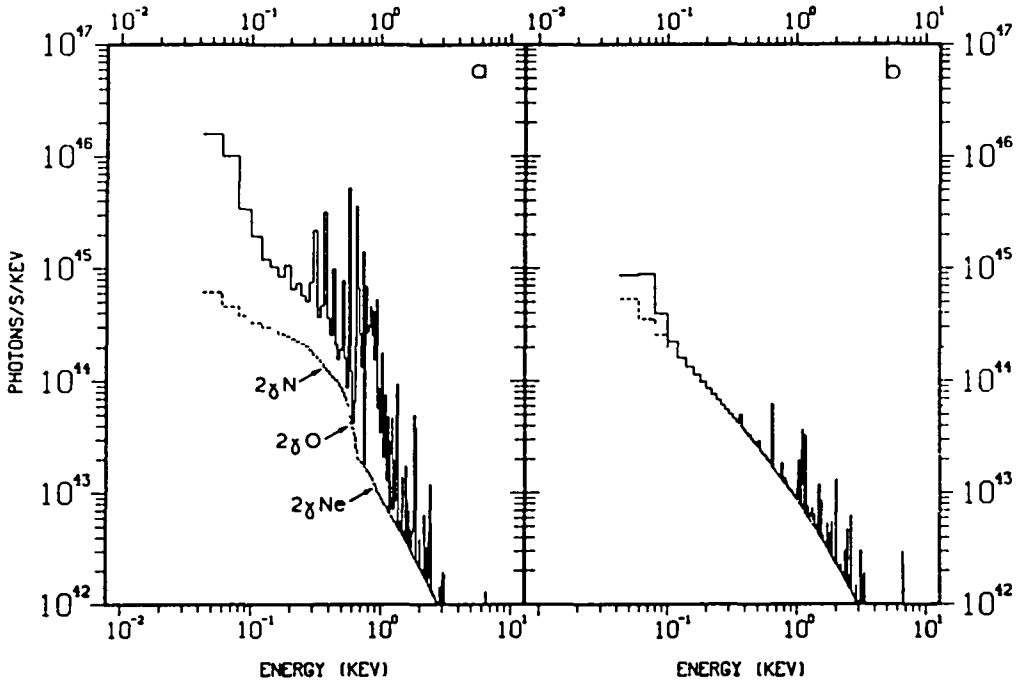

Figure III.7: A model spectrum for a remnant with (a) and without (b) the consideration of time-dependent ionization, taken from Gronenschild and Mewe (1982). The solid line is the full, line plus continuum spectrum; the dashed line the underlying continuum alone.

spectra of remnants, including a numerical hydrodynamic model for predicting the emission from hot ejecta in remnants like Cas A. One important contribution, used by subsequent workers, was his realization that the Coulomb heating of the electrons can be accurately approximated by a form which can be placed into the self-similar form of the Sedov solution. In the case of heating by multiple Coulomb scattering, the

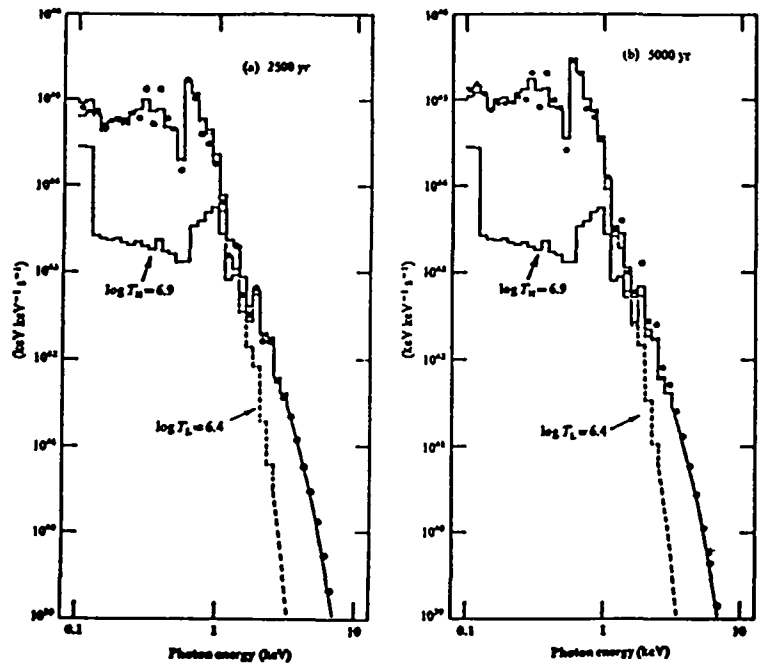

Figure III.8: The points are model spectra for two nonequilibrium remnants; the histograms an approximation based on the sum of two equilibrium components. Taken from Itoh (1979a).

electron temperature, T_e, obeys:

$$\frac{dT_e}{dt} \propto n\,(T-T_e)\,(\ln \Lambda)\,(T_e)^{-3/2},$$

where T is the average temperature, n the density, and ln Λ the Coulomb logarithm (Spitzer 1978). By neglecting the small variations in the

Coulomb logarithm over the range of densities and temperatures in the remnants, and substituting an appropriate constant value, the electron heating will scale with the rest of the remnant parameters. The electron temperature rises towards a plateau in the interior of the remnant, as the medium is so tenuous in the interior that the electrons are no longer heated. The maximum electron temperature attained in these models is ~1.5 keV, so that observations of higher temperatures in Sedov remnants indicates that other processes are heating some of the electrons. More recently, calculations of non-equilibrium remnants have been performed by Gronenschild and Mewe (1982), Shull (1982), Hamilton (1983), and Nugent (1983).

The current shock temperature and radius of a remnant in the adiabatic stage is determined by the parameters E/n_0, and t. To specify the rates for the equilibration of the electron and ionization temperatures, which are both proportional to density, requires the introduction of a third parameter. Combining three parameters that specify the remnant with the distance (and any interstellar absorption) completely determines the appearance of the remnant at the Earth.

We will try to determine the four parameters of the remnant from the available observables; the angular size, the magnitude of the X-ray flux, and the form of the X-ray spectrum. In a few cases, there are indications as to the distance of the remnant. The age is known for the few historical remnants, although their youth usually precludes them from having yet advanced into the adiabatic phase.

The three parameters that specify a Sedov phase remnant can be rearranged into two that specify the spectral shape and a third that supplies the normalizations for the size and flux. One choice for the pair that specifies the spectral form is the current shock temperature, T_{shock}, and $n_0 t$, the product of the density of the ambient medium with the age. This second quantity, $n_0 t$, indicates how quickly the shocked plasma attains equilibrium. Another choice for that parameter is $\eta \equiv n_0^2 E$, which rather than involving the unknown age, contains the explosion energy, E, which appears to be consistently in the range of $\sim 10^{50.5-51.5}$ ergs. As with $n_0 t$, larger values of η indicate that the plasma approaches equilibrium faster.

We will be using the models of the X-ray spectra from the time dependent ionization in adiabatic phase remnants for fits to data from real remnants which occurred in situations obviously more complicated than those assumed for the models. The particular spectral shapes of the models are determined by the distribution of emission measures versus ionization time. Hamilton and Sarazin (1983) have calculated this distribution for many types of SNR models, including some that may apply to an inner shock that heats the ejecta, in addition to those for the outer shock in the ISM. Many, but not all, of these more complicated models yield an ionization time distribution quite similar to that of the Sedov models. Thus, these Sedov model spectra can adequately approximate those for situations not covered by the simplified assumptions under which they were calculated. Once the best fitting Sedov model is found, one must also consider the other types of models that could give a similar spectrum.

The presence of the enriched SN ejecta can modify the X-ray emission, particularly in the young remnants. Initially it was thought that the ejecta would trail behind the blastwave, cooling by adiabatic expansion. Later it was realized that the drop in density that had been present at the surface of the progenitor, sets up a rarefaction wave that moves inward (in a Lagrangian frame) and lowers the interior pressure in the ejecta. This rarefaction, coupled with the adiabatic expansion, lowers the pressure in the shell of ejecta until it is below that directly behind the blastwave. This pressure imbalance gives rise to a compression wave which moves into the ejecta, steepens into a shock, and re-heats the ejecta (McKee 1974). This reverse shock will give rise to another hot component which may produce X-ray emission. Although the existence of these two components has been invoked to explain the multi-component appearance of the X-ray spectra, it is difficult to model because of uncertainties in the density of the ejecta. In a frame moving with the ejecta, the deceleration caused by sweeping up material is equivalent to a gravitational field and the ejecta will behave like a heavier fluid balanced over a lighter one. Such a configuration of fluids is Rayleigh-Taylor unstable and it will most likely relax by forming compressed, outgoing "tongues" of ejecta. This will tend to produce dense clumps of ejecta material, which may be shot out with fair velocity. This effect has been numerically modelled by Gull (1975b) who suggested that this is how the optical fast moving knots in Cas A, with their non-standard abundances, were formed. If the ejecta clumps are very dense when shocked, the temperatures will be low and little X-ray emission produced. Some material may be evaporated off the clumps and there may be X-ray emission from the hot interface region around the

cooler cloud. If some of the ejecta clumps have low enough density to be shocked to X-ray temperatures, perhaps showing up on X-ray images, it will be difficult to determine their densities, since the X-ray emissivity of metal enriched material is quite sensitive to the degree of the enrichment (Long, Dopita, and Tuohy 1982).

IV. EXPERIMENT AND ANALYSIS DESCRIPTION

This work is primarily concerned with X-ray spectra obtained with the Solid State Spectrometer (SSS) onboard the HEAO-2 satellite, which was christened the Einstein Observatory as it was launched during his centennial year. A description of all the instruments on HEAO-2 can be found in Giaconni et al. (1979). Here we describe aspects of the SSS relevant to our observations of supernova remnants; for other information on the instrument, see Holt (1976) for a general discussion of this type of spectrometer, and Joyce et al. (1978) for specific details of the HEAO-2 instrument.

Prior to HEAO-2, most extra-solar X-ray observations were performed using detectors with collecting area limited by the physical size of the instrument. Most of these detectors were gas-filled counters, in which the incident X-ray knocks an electron off one of the gas atoms by photoelectric absorption. This electron then ionizes other gas atoms, leaving a trail of ions and electrons. These electrons are then accelerated in an electric field set up by wires in the detection volume. During this acceleration, the electrons ionize more atoms, and create a shower which is collected onto the wires and measured. The field strengths and distances are chosen so that the shower does not reach saturation, so that the amount of charge collected is proportional to the energy of the incident X-ray. In addition to a number of non-ideal effects, the energy resolution of such a detector is determined by the statistics of the process changing the energy of the X-ray into the primary electrons, which is determined by the ionization potential. Such a detector, filled with a gas with an ionization potential of ~30 eV, can yield a FWHM resolution of ~400 eV at energies ~1 keV, when

allowing for the imperfect collection of charge. The sensitivity of these detectors is limited by the particle-induced background, which for a particular shielding and anti-coincidence scheme, scales with the detector volume.

To increase the ratio of signal to particle background noise and improve sensitivity requires a device to gather X-rays over a large aperture and bring them to bear upon a small detector. This collecting area advantage allows the use of types of detectors which have higher spectral resolution than would otherwise be available. HEAO-2 had an X-ray telescope, using Wolter type I grazing incidence optics, to serve as a collector for a variety of X-ray detectors which could be rotated into the focus.

In principle, the SSS functioned in a similar manner to the gas counters described above: an incident X-ray separated charges which were collected by an electric field. In a solid state detector, charge is created by the incident X-ray energy as electron-hole pairs in a semiconductor, rather than as electrons and ions in a gas. As the energy to promote an electron across the band gap is much less than the typical ionization potential, many more carriers are made, and better energy resolution is possible since the variance due to electrons lost to competing effects will scale as their number. Since solid state detectors do not have any type of internal low-noise amplification similar to the electron multiplication in the gas counters, the signals are very small, and real detectors do not achieve the resolutions indicated by the above analysis, but are limited by electronic noise in the external amplifiers.

The SSS used for these observations was a 9 mm diameter, 3 mm thick silicon wafer, with two concentric grooves machined onto the back, defining a central 6 mm diameter detector, and an annular guard ring which kept the field lines perpendicular to the face of the detector. The active volume of the detector was determined by the depletion depth of the reversed biased p-n junction. The depletion depth of a p-n junction increases with bias voltage until, at some point, breakdown occurs. To increase this depth, lithium, which serves as a mobile donor, was drifted into the p-type region to compensate for the acceptor concentration. The front face of the wafer was coated with gold which served as the electrical contact for providing the negative bias. This contact, with a nominal thickness of 50 Å, was clumped into irregular filaments. The detector was placed slightly out of the focal plane, so that the image of a point source would blur to about 1 mm and average over the surface irregularities. At this location, the detector had a flat top, circular beam of radius ~3 arc minutes, falling to zero response in ~1 arc minute. Before an X-ray could reach the detector, it must not have been absorbed by the telescope mirrors, by the aluminum coated parylene UV shield, by the gold contact, or by the "dead" layer of silicon above the active volume. The "windows" caused the effective area of the detector to be lower for soft X-rays. The Wolter Type I optics of the telescope focused the incident X-rays by two grazing incidence reflections. At the grazing angle determined by the length of the HEAO-2 satellite, the X-rays began to be absorbed by the mirrors above ~2.5 keV. By ~4.5 keV the effective area was down from the peak of ~200 cm^2 by over an order of magnitude.

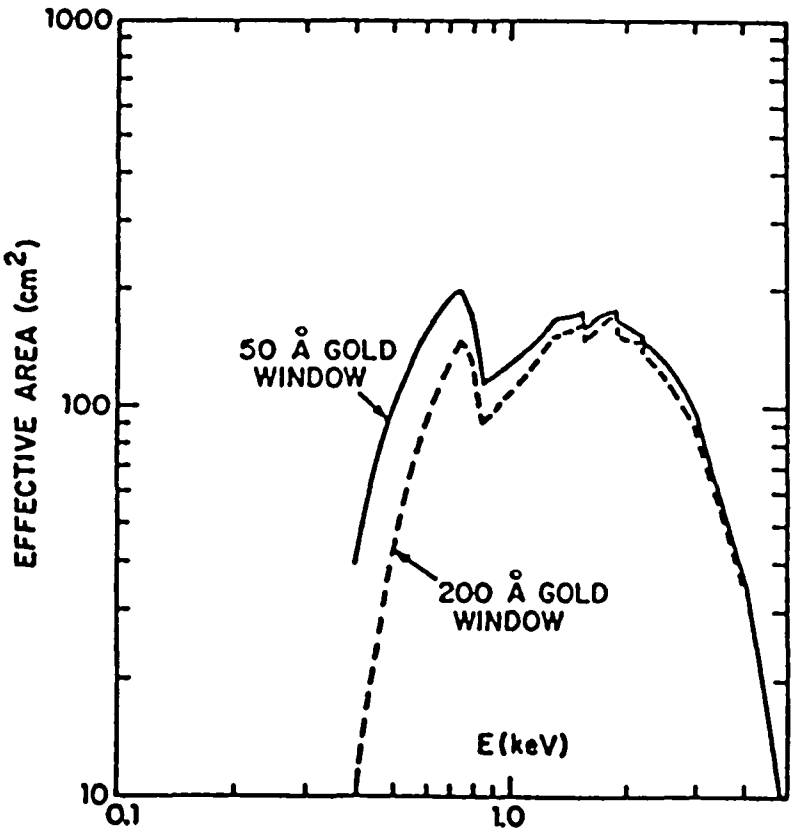

Figure IV.1: The effective area of the Solid State Spectrometer.

The energy-dependent effective area achieved with the SSS is shown in figure IV.1. One advantage of non-dispersive spectroscopy over dispersive spectrometers is that the entire bandpass is covered at one time; with a crystal spectrometer one can only measure within a small band and must build up spectra by splicing together many small pieces. In addition to this multiplex advantage, the efficiency of an SSS is much higher than spectrometers that depend upon reflections. For these reasons, the SSS was able to obtain more fields and extend to fainter objects than the higher resolution instrument on the Einstein Observatory, the Focal Plane Crystal Spectrometer (FPCS).

In order to reduce the number of thermally excited carriers, so that

the only charges to be collected are those created by the X-rays, the detector was cooled to ~100 K in a cryostat filled with solid methane and ammonia. This is below the optimum operating temperature for the Field Effect Transitor (FET), which must be kept physically close to the detector to minimize the noise contribution from the lead capacitance. The FET, connected to the detector only by a wire with low thermal conductivity, was left on at all times, so that it would be constantly maintained near the proper temperature.

A Light Emitting Diode (LED) was placed in the light-tight enclosure behind the detector wafer, that could illuminate the FET junction. When the LED was pulsed, the FET would conduct and let current flow from drain to gate to cancel the accumulated charge. This scheme avoids the noise from the feedback resistor that is conventionally used to regulate input bias. The LED was pulsed whenever the input bias rose above a set threshold, disabling the detector for less than 40 msecs. The firing rate of the LED was determined by the leakage current and gave some indication of the flux of charged particles.

Following the FET, the signal from the central detector was shaped and amplified in two parallel channels. The "fast" channel, with rise times commandable in the range 0.6-4.0 μsec, was used for pulse pile-up rejection and total rate information. The quieter "slow" channel, with commandable rise times from 6 to 40 μsec, provided the signal to the pulse height analyzer, which assigned one of 256 pulse heights spaced linearly to ~10 keV. In the nominal telemetry mode, only events in the first 128 channels were accumulated.

The unavoidable noise of the amplifier dominates the uncertainty of

the pulse height assignment, and would cause a monoenergetic signal from a perfect detector to yield a Gaussian of width (FWHM) ~160 eV centered on the proper pulse height. The statistics of the charge creation and collection add a term to the response so that the Gaussian has FWHM at energy E of $\Gamma(E)=[(160\ eV)^2 + 3.15 \times E(eV)]^{1/2}$.

The response of the detector has components other than the expected Gaussian centered on the incident X-ray energy. There is some probability that during the conversion of the X-ray a silicon atom will be excited which will then fluoresce and emit a characteristic X-ray which can exit from the detector. The energy left to be measured in the detector will, for a mono-energetic input, produce a secondary peak, often called the escape peak, at a pulse height lower than the incident energy by 1.739 keV, the energy of the escaping X-ray. In addition to the primary peak and the escape peak, an incident X-ray can produce, with low probability, any pulse height less than the one corresponding to the incident energy, due to other loss processes. This gives a low level pedestal, which will be important when fitting spectra from hard sources, or sources with very large amounts of material in the line of sight, which will absorb the softer X-rays.

Several parameters of the in-orbit performance had to be determined post-launch. The calibration of the system gain was obtained from PHA taken while the detector was viewing a ^{55}Fe source, located on the cover of the experiment. As the two lines produced by the calibration source fall outside of the normal range of the telemetry, the calibration mode returned the uppermost 7 of the 8 bit PHA rather than the standard least significant 7, effectively dividing the output by two. The coefficients

for a linear model of the detector gain were determined by fitting these calibration lines. The gain parameters would have been better determined if a calibration source with more widely separated lines had been used. We adopted gain parameters modified from the calibration data to minimize the deviations in a thermal equilibrium model to the bright lines in Cas A. During these investigations, an additional small shift in the gain offset was adopted which improved the fits.

The detector response is modelled as a matrix, used to multiply a model spectrum to yield a model of the pulse height data that spectrum would produce. The parameters used to generate the matrix were adjusted to yield a good fit to data taken from the Crab nebula when starting with the assumed spectrum of the nebula. Initially, a matrix was constructed using the adopted gain parameters (not including the final small offset term that was added later), parameters for the thicknesses of the various absorbing layers, a model for the shape of the two peaks and the pedestal, and a model of the area of the telescope versus energy. This matrix was then used to generate a trial vector, assuming that the Crab has a power law spectrum with index 2.13 that is absorbed by cosmic abundance material having a column density 3×10^{21} equivalent hydrogen atoms cm^{-2}. The energy-dependent telescope areas were then changed by the ratio of the real data to the trial vector, a new matrix was generated, and the process was repeated. After four iterations, the process was stopped as the reduced chi-squared of the trial fit was marginally acceptable.

The detector shared a common vacuum with the multi-layer insulation-filled space between the inner and outer walls of the cryostat. After the system was sealed, some material, probably water vapor outgassed from the multi-layer insulation, was cryo-pumped onto the detector surface. In orbit, the detector was heated to drive off the condensate, but since there was no large vent to the outside (in order to keep external vapor from being cryo-pumped onto the cold surfaces), most of it immediately began to return. To account for this variable absorbing layer in front of the detector, we developed a model to describe the return of the ice. The parameters for this model were derived from spectra of various bright, reasonably constant objects (primarily the Crab Nebula) taken at various times after the defrosts. These spectra were compared and the form of the absorption was found to be consistent with a variable column density of oxygen atoms. It appeared that the ice did not form an even layer, but accumulated in clumps. To account for the clumping, parameters for the fraction covered versus amount of ice were developed. The model of the ice appears to be fairly reliable. At times during model fitting a free parameter is introduced to allow for a variation from the modelled amount of ice. This is usually only necessary if the column density of interstellar material in the line of sight is being held fixed at some known value, as otherwise a change in the interstellar column is able to mimic the difference in ice thickness.

The accumulated PHA spectra include background events. The rates of the background events were determined for a group of blank sky observations. After attempting to correlate the background rates with satellite position and other rates available in the spacecraft, two

components of background were identified. The first background component was correlated with the rate of events that exceeded an upper threshold on the "fast" channel. This component, properly normalized for this rate and the exposure length, is automatically subtracted from the data by the display and fitting software. The other component of the background has the form of an enhancement at ~3.5 keV, as well as some excess counts in the lowest channels similar to the other component. This bump may be caused by signal induced in the central volume by alpha particles passing through the periphery. This component does not appear to correlate with any of the variables examined. As this component has a fairly distinctive shape, its strength can be well estimated by adding a template bump to the model being fit, and adjusting the normalization until the best fit is obtained. These background subtraction schemes are adequate for moderately bright sources, but some caution is necessary in interpreting features near 3.5 keV in spectra from weaker sources. In particular, there is some evidence that the shape and location of the bump was variable, so that subtracting the template bump can create spectral features.

Data Analysis

The telemetry stream from the SSS was formatted into records corresponding to each 2.56 seconds of data and stored on tape. The PHA spectra are collected from these records with a program that examines each record for various (adjustable) data quality criteria and accumulates spectra and average rates for background subtraction from the accepted records.

The rows of the detector matrix have a large number of non-zero elements, corresponding to the large range of PHA channels that can be incremented by a monoenergetic beam. The matrix is therefore ill-conditioned; a straightforward attempt to obtain the incident spectrum by multiplying the observed PHA spectra by the inverse of the response matrix cannot work in the presence of the statistical noise which will always be present in a physical detector. We implemented some procedures (Blissett and Cruise 1979, Kahn and Blissett 1980) for obtaining an approximation to the inverted spectrum by expanding the system in a set of eigenfunctions appropriate for the particular response matrix and data and filtering out the power that would correspond to the high frequencies in a more conventional Fourier expansion. These procedures hold promise for enhancing features not apparent to the eye in data taken with detectors with poor spectral resolution. There did not appear to be a large advantage to applying these techniques to the SSS data, as it required filtering that produced an estimate of the incident spectra with an effective resolution no better than that of the initial data.

The inversion techniques can indicate what features a model spectrum should have, but cannot supply accessible quantitative information on the strengths of such features. Estimates of the values of model parameters were obtained by adjusting parameters of models to minimize the difference between the model PHA spectra and the data. That difference is measured by a form of the conventional χ^2 statistic using the standard deviations of the data points rather than the deviations predicted by the model. For most of the models reported here, we do not achieve a numerically acceptable fit. One factor contributing to the

inability of the models to acceptably reproduce the data was the absence of some transitions and elements from the models available to us. Another contribution comes from the uncertainties in the atomic physics data used to calculate the lines. Some contribution comes from the uncertainties in the model of the detector response. We were unable to correct for these various contributions, and could not easily estimate their magnitude.

Allowed ranges of model parameters are found using the procedure outlined in Lampton, Margon, and Bowyer (1976). The value of the parameter is stepped away from its best-fit value, while leaving all other parameters free to vary, until χ^2 increases by an amount corresponding to the significance level of the range being quoted. The best fitting parameter values are found using a modified version of the Bevington (1969) realization of the Marquardt (1963) gradient-expansion algorithm.

The fitting and display software requires models of the spectrum incident on the telescope evaluated at the energies for which the columns of the detector matrix were constructed. The number of columns must be kept as small as possible to reduce the computational requirements. The detector matrix used here had 150 columns, spaced by 36 eV, with the center of the first column at 295.3 eV. This spacing is large compared to the precision with which the SSS could determine the centroid of a bright line, so the flux for a line was divided between two adjacent model bins in proportion to its position relative to the centers of the bins. This places the centroid of the resulting PHA spectrum at the proper energy, rather than placing all lines at the bin

centers. A similar procedure is necessary for treating the position of an absorption edge within a model bin. The programs allow models to include various combinations of emission and absorption processes. The model for the photoelectric absorption of X-rays by material in the line of sight uses the compilation of Brown and Gould (1970) with the addition of iron from Fireman (1974). Various types of simple continua, such as power law, thermal bremsstrahlung, and black body are available but for this research we often used spectra too complex to be calculated within the fitting program. These spectra were calculated once at set values of their model parameters and stored away for later use by the fitting programs. The programs can interpolate between adjacent models, producing an approximation to the spectra that would be produced for values of the parameters intermediate to those calculated originally.

There were four sources for the stored models we used in this investigation. There were actually multiple versions of most of the models as we worked with the model builders to resolve various difficulties with their codes. Here we report results using the versions available to us as of ~1982. The estimates of many of the rates used in these codes are likely to be revised in the future.

For models of a thermal plasma in equilibrium, we use a modified version of the code of Raymond and Smith (1977) with updates as listed in Raymond (1978) and Pravdo and Smith (1979). We formed sums of these equilibrium spectra weighted by the emission measure of shells in the Sedov solution to generate estimates of the spectra that would be produced by adiabatic remnants in equilibrium. Spectra from models of adiabatic remnants with time-dependent ionization were provided to us by

Shull (1982) and Hamilton (1983; also described in Hamilton, Sarazin, and Chevalier 1982). Shull calculated a range of T_{shock} for an explosion with $\eta=10^{51}$ ergs cm^{-6}, and assumed that the electrons equilibrate with the ions near the shock. Hamilton calculated over a range of both T_{shock} and η, once assuming that the electrons immediately equilibrate, and once assuming that the electrons are only heated by Coulomb collision.

V. VARIATIONS IN X-RAY SPECTRA ACROSS PUPPIS A

There are several advantages to studying Puppis A before addressing younger remnants. It is sufficiently old so that it might be possible to use adiabatic expansion phase models, which are determined by fewer parameters than the models for younger remnants. During the several thousand years since the explosion, it has expanded to a size which, when viewed from our relative proximity (~2kpc), presents a projected angular diameter (~50 arcmins) large enough to permit several independent fields of view for instruments with moderate spatial resolution. The amount of material swept up during the expansion would have diluted the ejecta so that the emission should not be complicated by the effects of high metallicity. The remnant has been well studied in other wavebands as well as by the previous generation of X-ray detectors.

Previous Observations

In the initial optical observations, Baade and Minkowski (1954) found large [NII]($\lambda\lambda$ 6548 Å, 6584 Å) to Hα ratios, which varied from filament to filament. Dopita, Mathewson, and Ford (1977) found slight traces of other elements, but confirmed the high abundance of nitrogen. Their models for the shocked material require nitrogen to be enhanced by at least a factor of ~10 to fit the optical spectra. Oxygen and sulfur were enhanced by at least a factor of 2 relative to hydrogen in that filament. The shock model giving the best fit to the spectra had a pre-shock density of 120 cm^{-3} with a post-shock temperature of 72,000 K, although determination of temperatures and densities from these optical spectra are uncertain due to the unusual abundances. Kirshner and

Winkler now report (1982) that the some of the knots of Puppis A show very strong oxygen lines as is seen in some of the quasi-stationary flocculi of Cas A.

Lucke et al. (1979) have observed the remnant in the 5303Å line of [Fe XIV] and the 6374Å line of [Fe X]. Their upper limit for the Fe X/Fe XIV line ratio indicates that, assuming coronal equilibrium, the plasma must be hotter than 1.8×10^6 K. Their absolute flux for Fe XIV emission, which arises in gas at 2×10^6 K, was too low to be reconciled with the emission measure deduced for the observed soft X-ray component, under any model that assumes the gas to be in thermal equilibrium.

In the radio, the remnant appears as an incomplete shell with several bright spots along the circumference (Milne 1971, Green 1971, and Milne et al. 1983). The spectral index of $\alpha \sim -0.53$ (from 408-5000 Mhz) is approximately constant across the remnant. The radio emission is not correlated with the optical emission. The intensity-weighted average polarization at 5 Ghz is 3.1%. In the radio-bright eastern edge the polarization angles correspond to a radially oriented magnetic field.

Previous X-ray Observations

The early X-ray observations of Puppis A are summarized in Zarnecki et al. (1978). The various determinations of temperature and intervening column density from these measurements were mutually inconsistent. Zarnecki et al. attempt to reconcile these differences with a model in which the X-ray spectrum is formed by two components with temperatures of 2.5 and 12.6 times 10^6 K. They identify the lower

temperature with a bright region on the eastern edge of the remnant, where an early crystal spectrometer experiment detected emission from O VIII (Zarnecki and Culhane 1977). This region of the sky has a high density of X-ray sources and it is difficult for the proportional counter experiments to isolate Puppis A above ~5 keV, so there is limited information available concerning the high energy spectrum and the maximum temperatures attained by the electrons.

Extensive observations of Puppis A were obtained by the instruments of the Einstein observatory. Petre et al. (1982) produced the high resolution map used in Figure V.1. They find a complex structure presumably reflecting the inhomogeneities of the ISM. They suggest that the ISM has many regions with sizes in the range 0.1-5 pc with density enhancements of approximately a factor of two, and that the brightest X-ray features arise in two isolated clouds, one of which corresponds to the soft region of Zarnecki et al. From the surface brightness, they estimate the densities of the clouds at ~10-30 cm^{-3}, approximately ten times more dense than the bulk of the X-ray plasma.

The focal plane crystal spectrometer (FPCS) made high resolution spectral observations of some of the lines of oxygen, neon, and iron (Winkler et al. 1981a, Winkler et al. 1981b, Canizares and Winkler 1981). By measuring the ratio of lines arising from the same ionization state in oxygen, the FPCS investigators could determine the column density of material along the line of sight to be 4 ± 2 times 10^{21} atoms/cm^2. They interpret their line strength measurements as showing enrichment of oxygen and neon relative to iron, and take this as evidence for the X-ray plasma containing some ejecta of a Type II SN.

The SSS Observations

Table V.1 is an observing log for the eight fields that the SSS observed within the Puppis A SNR. These positions are indicated on the HRI photomosaic of Petre *et al.* in Figure V.1. The spectra, corrected for varying amounts of absorption due to water cryo-pumped onto the detector, were compared by subtracting each one, properly normed, from another, and when no significant differences were found, the similar ones were combined. The three adjacent fields across the interior were combined into the spectrum labeled "I". The western-most two and the southern-most one were combined into the spectrum labeled "R" for rim. The spectrum from the field on the eastern bright spot is labelled "C" for cloud, and that from the northern interior field is

Table V.1: The SSS observations of Puppis A. Field name, Right Ascension (1950) in hours, minutes, and seconds, Declination (1950) in degrees and arcminutes, the net time in seconds, and the raw counting rate in counts per second.

Field	R.A.	Dec	Time (secs)	Rate (cts sec^{-1})
I1	8 22 00	-42 45.0	2621	4.76
I2	8 21 30	-42 45.0	4178	5.63
I3	8 21 00	-42 45.0	9953	3.46
N	8 21 00	-42 37.5	2990	3.64
C	8 22 25	-42 47.0	4833	5.46
R1	8 18 50	-42 50.0	1638	0.88
R2	8 19 45	-42 38.0	5652	0.74
R3	8 22 30	-42 56.0	6267	2.25

labeled "N". These spectra, seen in Figure V.2, each show obvious line

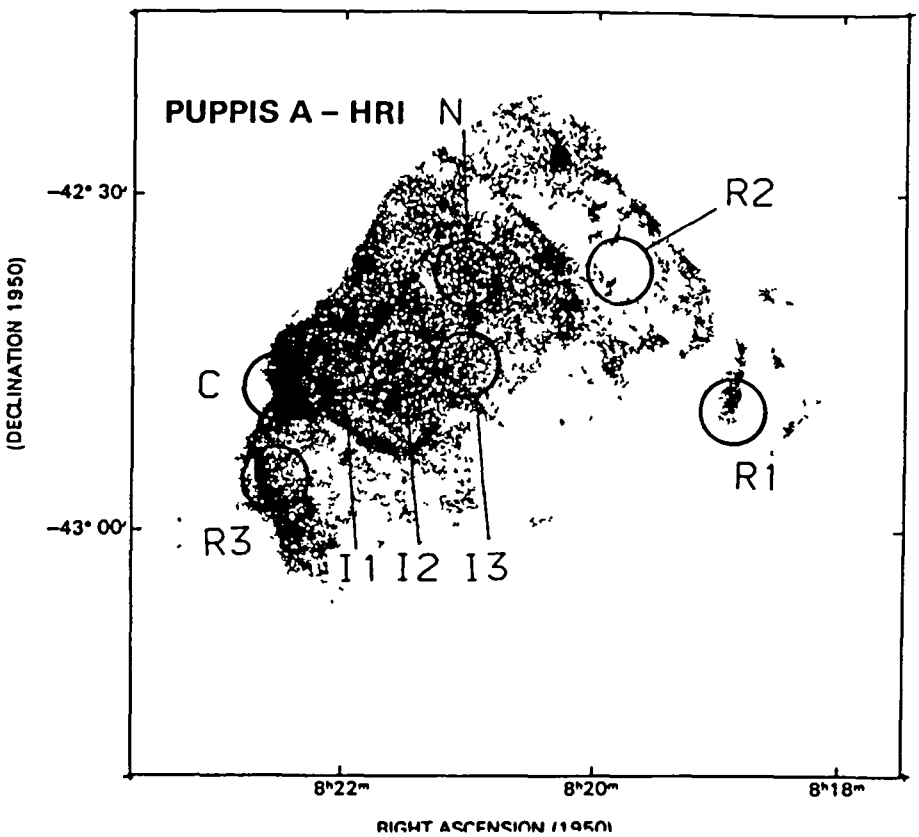

Figure V.1: The positions of the SSS observations placed on the photomosaic of Petre et al.

features from the helium-like ion stages of magnesium, silicon, and sulphur. After checking that there did not appear to be any differences in the SSS spectra obtained at different locations due to changes in the amount of absorbing material, we adopted the FPCS value for n_H, 4×10^{21} atoms/cm^2, for our analysis.

The most obvious differences among the four spectra are the large equivalent widths of the lines in spectrum N and the soft excess in spectra C and R. We attempted to fit the soft excess by models involving an absorption change or the enhancement of a single line

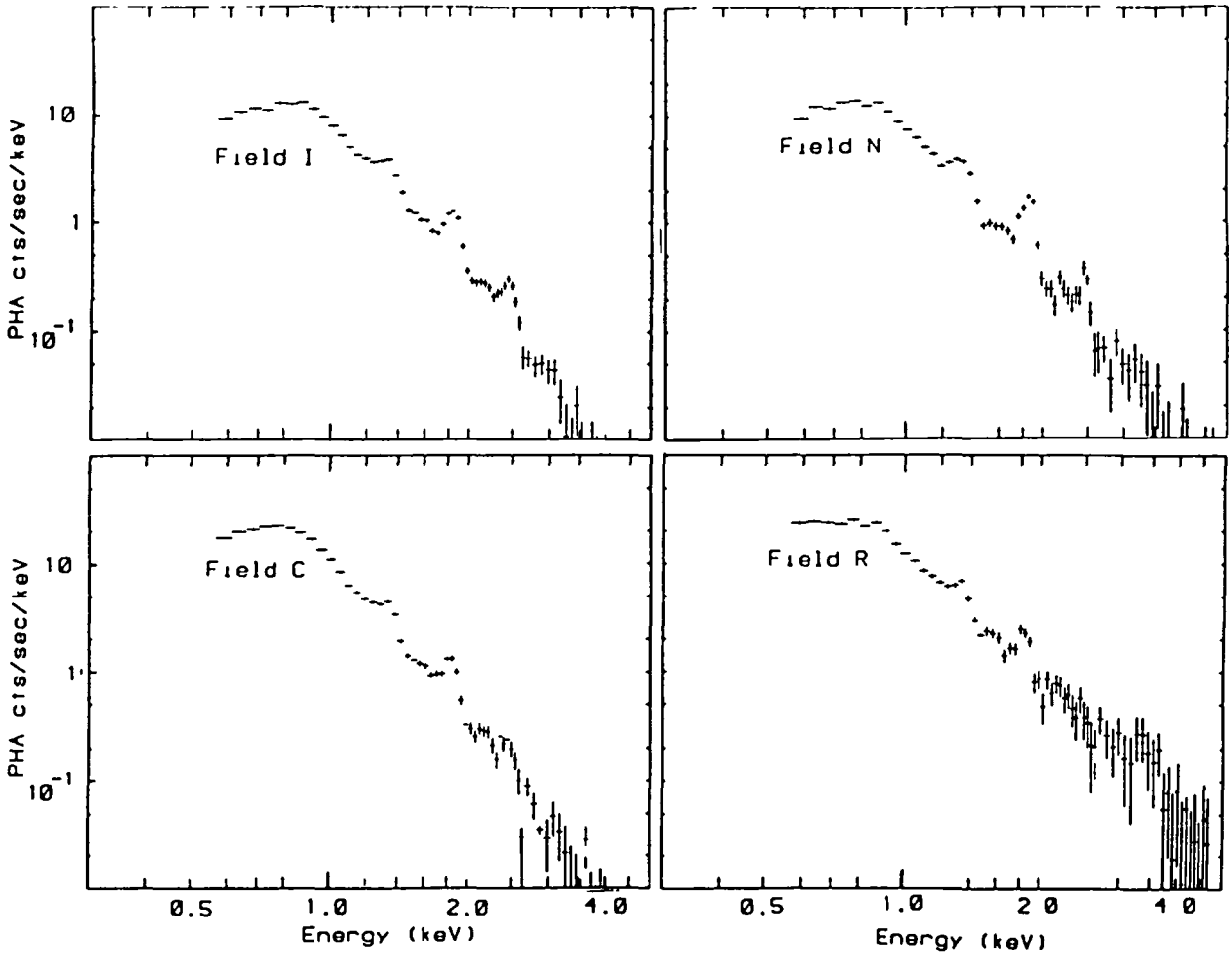

Figure V.2: The SSS spectra, corrected for amount of ice on the detector.

intensity. Neither model could provide acceptable fits.

To facilitate comparison with earlier works and other remnants we first present results from over-simplified models with a single component in thermal equilibrium. The parameters from these models are listed in table V.2. In no case do "cosmic" abundances yield an acceptable fit. All four models have a temperature lower than 0.5 keV in contrast to the ~1 keV obtained over the higher energy range of the

proportional counters. As discussed in Chapter III, multiple equilibrium components can be used to mimic the spectra produced by a model in which the time-dependent ionization of the plasma is considered. The abundances in these fits increase with the atomic number for the elements producing K lines within the SSS bandpass. It is unlikely this actually reflects the abundances in the remnant, and is also probably due to the non-equilibrium ionization. The best fit temperatures are low in order to produce sufficient emission from oxygen and iron and to avoid overproducing the lines from the hydrogen-like analogues. In an equilibrium plasma at these temperatures the heavier elements are under-ionized and high abundances are required in order to produce bright enough lines. Figure V.2 illustrates how the various

Table V.2: Parameters for single temperature models.

Field	I	N	C	R
Temperature (keV)	0.32	0.32	0.52	0.29
Abundances				
Ne	5.52	2.58	0.07	2.58
Mg	4.98	1.80	0.23	1.80
Si	14.5	6.66	0.39	6.66
S	118	53.0	0.92	53.
Ar	46	19.2	0.02	19.2
Ca	24	45.5	69.9	45.5
Fe	2.16	1.50	0.69	1.50

elements can not all be in the helium-like state at any temperature in an equilibrium plasma and, as this configuration is likely in an ionizing plasma, provides another indication that non-equilibrium models should be considered. Another effect is also responsible for the large

abundances of argon and calcium in these models. Large argon and calcium lines can be used, due to the resolution and counting statistics of the data, to reduce the discrepancy between the fall off of the continuum at high energies, due to the low temperatures of these models and the high energy excess in the data, which is the beginning of the hotter component seen by higher energy experiments.

Next we performed fits with models having two components which were each separately in thermal equilibrium at different temperatures. With the abundances in each held at solar values, we obtained the results presented in Table V.3. Note that while the temperatures obtained for the two components are approximately the same in all four spectra, the ratio of the emission measure in these components varies. In the

Table V.3: Temperatures (keV) and the ratio of the emission measures for two component models.

Field	I	N	C	R
T_{low}	0.20	0.20	0.20	0.19
T_{high}	0.57	0.54	0.59	0.54
E.M. Low/High	4.8	6.0	9.3	12.7

multi-component model of Zarnecki et al. (1978), the low temperature component was believed to arise only from the bright region on the eastern edge. Our fields, far from this bright spot, still require some low temperature component. The soft excesses in spectra R and C require a larger amount of emission from the soft component. The value of the higher temperature was driven by the small counting statistics on the large silicon lines; it is the temperature at which the silicon in a

solar abundance plasma in coronal equilibrium has the largest helium-like lines.

In order to apply more sophisticated models, we formed diagnostics from the line strengths measured by the SSS and FPCS. The lines in the SSS spectra are sufficiently strong compared to the continuum so that errors in determining the continuum level do not cause significant errors in the derived line strengths. The line strengths in Table V.4 were obtained by fitting individual narrow lines above the continuum provided by a best fitting model, after the element whose lines were being measured was removed from the model.

To determine the abundances in the plasma from line strength

Table V.4: Line strength ratios

Field	I	N	C	R
1-4.5 keV Flux (phots/cm^2/s)	2.3(-2)	2.0(-2)	2.6(-2)	6.1(-3)
Si Heα/Flux	0.10±0.01	0.15±0.02	0.07±0.01	0.07±0.02
Si Heβ/Heα	0.14±0.02	0.08±0.02	0.26±0.06	0.30±0.06
Si Lyα/Heα	<0.09	<0.05	<0.08	<0.15
Mg Heα/Si Heα	2.6±0.2	2.1±0.4	2.4±0.4	2.6±0.8
S Heα/Si Heα	0.26±0.04	0.18±0.06	0.19±0.07	0.2±0.1

measurements requires the emissivities for each line. The emissivities are determined from estimates of the the electron and ionization temperatures. The temperatures will not necessarily be identical because, as was discussed in Chapter III, it may take longer than the

age of Puppis A for the plasma to relax to equilibrium. In addition to the calculations which indicate that remnants as old as Puppis A may still show non-equilibrium effects, there are previous observations of Puppis that indicate that no single-temperature equilibrium model can suffice. As mentioned above, the proportional counter observations have required models with at least two temperatures. The enhancement of two-photon continua and line radiation in the 0.1 to 1.0 keV range in a homogeneous non-equilibrium SNR will produce an X-ray spectrum with a two-temperature appearance (Gorenstein, Harnden, and Tucker 1974; Itoh 1979a; Gronenschild and Mewe 1982). While multiple temperatures may be expected in fits to the proportional counter data which are averaged over large areas of the remnant, the FPCS obtained different ionization temperatures from several line ratio diagnostics within a fairly small slit (3×30 arcmins). There is optical evidence that the apparent low X-ray temperature cannot arise from a component in thermal equilibrium. Lucke et al. (1979) could not reconcile the weakness of their measurements of the coronal Fe XIV 5303 Å line with the X-ray derived volume emission measure of the low temperature component, which should have produced the coronal line if in equilibrium. Itoh (1979b) showed that the line strengths predicted in a non-equilibrium remnant model could be of the same order as those measured by Lucke et al.

In addition to indications of ionization temperatures, FPCS line measurements can provide constraints on the electron temperature. It is difficult to determine the electron temperatures from the ratios of lines from different ionization states, but taking ratios of lines from the same ionization state removes the dependence on ionization temperature. The expression for the ratio of the fluxes at the detector

of the lines from a state (designated as "i") to the ground state ("g") and from another state ("k") to the ground state is given by:

$$\frac{F_{ig}}{F_{kg}} = \frac{\Omega_{ig}\ e^{(E_{kg}-E_{ig})/kT_e}\ e^{n_H(\sigma_{E_{kg}}-\sigma_{E_{ig}})}}{\Omega_{kg}} \quad ,$$

where Ω is the effective collision strength, σ_E the photoelectric absorption cross-section for the interstellar medium, n_H the column density in the line of sight, and E_{ig} and E_{kg} the energies of the two transitions. Since the oxygen lines measured by the FPCS are relatively close together in energy, the dependence on T_e is small, particularly as n_H is uncertain. Any $T_e > \sim 1.5 \times 10^6$ is permitted, without resorting to unreasonable values of n_H.

The SSS could determine ratios of some lines from the same ion stage which is the type of diagnostic required for determination of electron temperatures. These line ratios, labelled Heβ/Heα in Table V.4 are the ratio of the $1s^2$-1s3p line to the sum of the $1s^2$-1s2p triplet. Unfortunately the recombination rates and collisional excitation cross sections for the N=3 levels of the helium-like ions have not been accurately calculated, and we cannot yet interpret these ratios but make them available here against the day when the atomic physics calculations have been performed.

These particular diagnostics are not very sensitive in the non-equilibrium models. Figures 10 and 11 in HSC, which give Heα/Heβ and Lyα/Lyβ flux ratios for oxygen, show the ratios to vary by less than a factor of 1.6 over the T_{shock}-n plane, which covers over two orders of magnitude in shock temperature.

There are two more sets of measurements available which help to constrain the electron temperature. First is the 1 keV component seen in the proportional counter observations. Zarnecki et al. (1978) estimate that this component supplies ~20% of the X-ray emission, so it may not be neglected. As long as the assumption of adiabatic expansion in a homogeneous medium applies, at least locally, and there are no other processes, such as stochastic acceleration heating some of the particles, the hottest temperatures seen will supply an approximate lower limit to the shock temperature. Thus the measurements exclude the lowest shock temperature region of the T_{shock}-n plane. In the models in which the electrons are heated only by Coulomb collisions and not by some process in the shock, a 1 keV appearance implies a much higher shock temperature, unless the rate of Coulomb collisions is very large due to high densities.

The ratios of the three lines making up the Heα triplets can be used for electron temperature diagnostics (Pradhan 1982). From the ratio of the forbidden plus intercombination lines to the resonance lines in the Heα triplet in O VII, Canizares et al. (1983) find that the plasma in Puppis A has not reached an ionization state of coronal equilibrium, but is still ionizing in a bath of electrons with temperatures greater than 5×10^6 K.

The next diagnostic available gives limits to the ionization temperatures in magnesium, silicon, and sulphur. These are upper limits on the ratio of the strength in the Lyman α analog to the strength of the helium α triplet. The upper limits for this ratio in magnesium implies a temperature of less than 5×10^6 K for the plasma if in

equilibrium. At this low a temperature, a cosmic abundance plasma would produce smaller S XV lines than we observe. The low temperature also conflicts with the constraints noted above.

The FPCS measured similar ratios for oxygen and neon. These ratios would indicate an equilibrium ionization temperature of $2.2\pm0.2\times10^6$ K for oxygen and $\sim4\times10^6$ K for neon. Again the difference in two temperature diagnostics might appear to require multiple components but these line strengths could arise from a single component in a non-equilibrium model. The Heα/Lyα ratio in oxygen does not vary much over most of the T_{shock}-n plane, but the same ratio in neon is more sensitive. Figure V.4 shows the FPCS value for this ratio, plotted on the parameter plane.

If we assume that the plasma in Puppis A is relatively homogeneous within each of the fields making up one of the SSS spectra, we are lead to conclude that a non-equilibrium model is required. In addition to fitting our measured line strengths, we should consider the other information present in our spectra. Although individual lines cannot be resolved in the region from 0.5 to 1.3 keV we should be certain that our models are consistent with the spectra.

With some constraints on the ionization state of the elements in the plasma, appropriate emissivities can be used to invert our line strength measurements to abundance determinations. Combining the information available from the FPCS with that from the SSS shows that oxygen has a slight majority in the one electron state; neon is mostly in the two-electron state with perhaps one third in the hydrogenic state; and magnesium, silicon, and sulfur are almost completely in the two-electron

state. There is no equilibrium plasma that has this ionization distribution. Examining the non-equilibrium models of HSC shows however, that spectra from approximately this distribution can occur in a remnant with $T_{shock} \simeq 10^7$ K and an ionization time, $n_0 t$, less than ~6000 years cm^{-3}.

Before addressing the abundances in Puppis A we summarize the lines of evidence and reasoning that suggest that the abundances in Puppis A may be anomalous. The optical spectroscopy referenced above shows some of the filaments to be highly enriched, although the total mass in the optical filaments is quite small. The FPCS investigators have reported that their line strength measurements require an enhancement of oxygen and neon relative to iron (Canizares and Winkler 1981). The outer layers of an evolved 25 solar mass star contain material sufficiently enriched so that significant abundance anomalies will exist even after dilution with many solar masses of ISM.

We first consider the relative abundances of the elements producing the large lines in the SSS observations. Our best measured line ratios are shown in Figure V.4 along with several models. These figures are constructed so that the model points, which were calculated for a plasma with cosmic abundances, can be shifted to model a plasma with elemental enhancements. The vector from a model point to the data point indicates the change in the relative abundances required for that model to match the observed line ratios. The long arrow on the figure indicates the direction and magnitude in which the model points should be moved if the X-ray plasma had the abundances expected in the ejecta

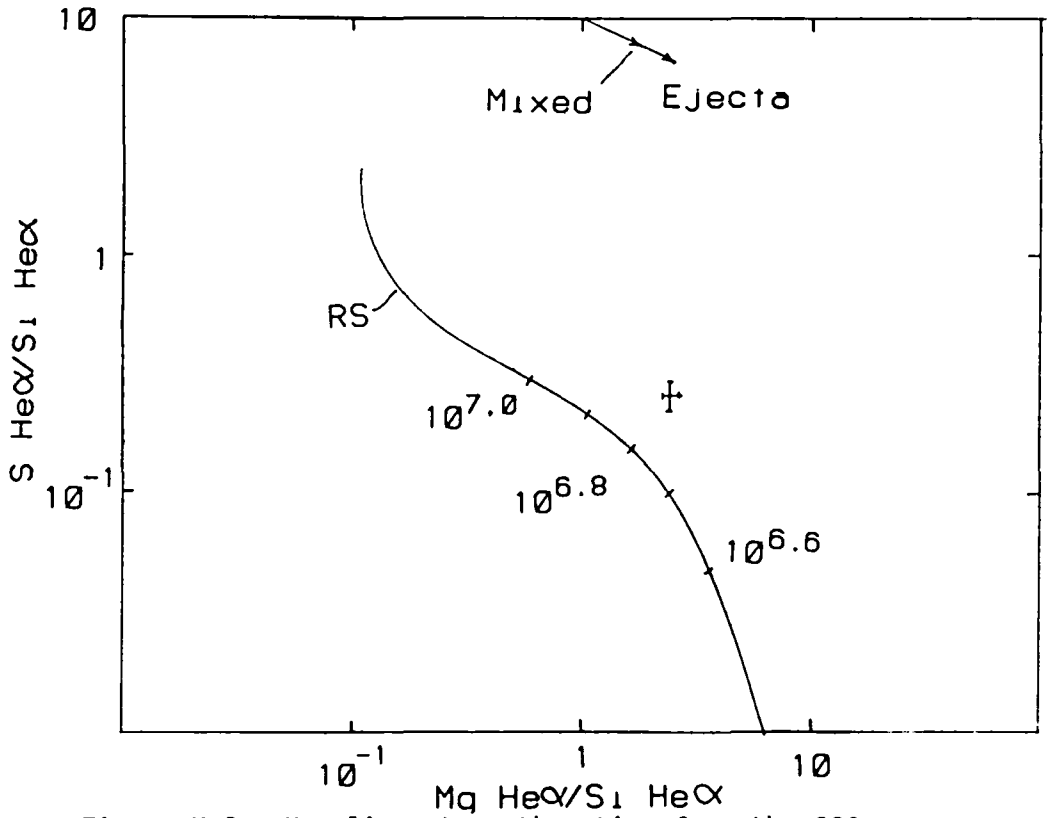

Figure V.3: Hea line strength ratios from the SSS measurement of field I. In this and the next figure the axes give line stength ratios for two pairs of three elements. Model points and curves are plotted for the ratios predicted for whichever measure of standard abundances the model builders adopted. The model points would be shifted to account for plasma of different composition than the standard. In each figure, the arrows indicate the shift which would be required for the abundances predicted for a Type II supernovae by Woosley and Weaver.

from a Type II supernova. The latter abundances were taken from Table 2 of Woosley and Weaver (1983) and are the pre-explosion abundances of a Population I 25 solar mass star; only small changes are expected due to nucleosynthesis during the explosion. The shorter arrow represents the enhancements for the ejecta from a 25 solar mass Type II diluted with 100 solar masses of ISM having cosmic abundances. The model curve labelled RS (Raymond and Smith 1977) is the prediction for a homogeneous

plasma in equilibrium, with labels giving the log of the temperature. Although moving the RS models to account for the possibility of enrichment reduces the distance between the models and the measurements, it does not bring the models close enough to be considered. The curves labelled I and G are taken from the calculations of Itoh (1979a) and Gronenschild and Mewe (1982). The other points are from Hamilton et al. (1983). While the equilibrium models require relative enhancements unlike those expected for a supernova, some of the non-equilibrium models yield line ratios quite near those observed when starting with cosmic abundances.

Figure V.4 is a similar illustration for lines observed with the FPCS. The ratios plotted were calculated for the fluxes given in Winkler et al. 1981b and are not the ratios given in Canizares and Winkler 1981, which the authors agree are in error. Included in Figure V.5 are the line ratios measured by Walker, Rugge, and Weiss (1974) for the quiescent solar corona. Canizares and Winkler claim that the offset of the solar point from their measurement, which is similar to the enrichment prediction shown by the arrows, is evidence for such an abundance enhancement. However, the non-equilibrium calculations using cosmic abundances predict line ratios close to those the FPCS measured in Puppis A. Some of this discrepancy could be due to non-equilibrium effects. In particular, Canizares and Winkler argue that since they do not observe lines from ionization stages other than Fe XVII, that line strength can be used as a measure of the total amount of iron present. The stability of the filled shell of neon-like Fe XVII causes this ion to predominate over a large range of temperatures in an

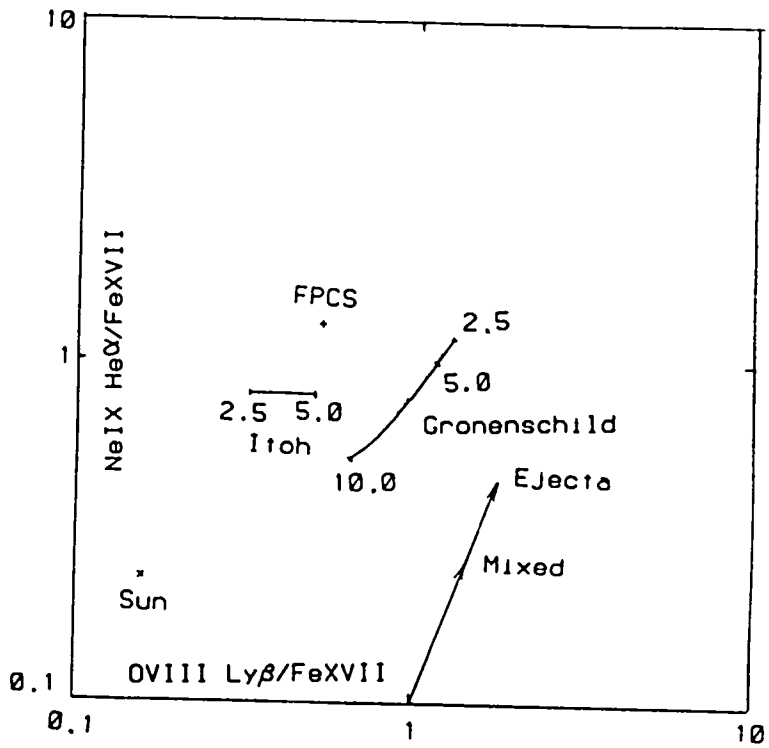

Figure V.4: Similar figure to previous one for FPCS measurements. The data point labelled "Sun" shows line ratios measured by Walker, Rugge, and Weiss for the quiescent solar corona. The curves marked Itoh and Gronenschild are labelled with the age (in thousands of years) of the remnants modelled in their papers.

equilibrium plasma and to be relatively long-lived in an ionizing plasma. But although Fe XVII is the ionization state with the highest fraction, and hence the brightest line, much of the iron behind a sufficiently fast shock will be distributed across a series of higher ionization states. There is not enough in any one of these states to produce large lines characteristic of those states. This may be seen, for example, in the distribution of ion fractions in the corrected version (the printed version has Figure 3f repeated) of Gronenschild and Mewe (1982) figure 2f. Similarly, Figure 14 of HSC shows that the lines

of the higher ionization stages of iron are diminished relative to those of Fe XVII, until large values of $n_0 t$. Thus the lack of lines from higher ionization states cannot be used as an indication that most of the iron is in the Fe XVII state, and that the Fe XVII line strength is a reliable measure of the total amount of iron present. HSC calculate the specific line ratios used by the FPCS authors. At no point in the T_{shock}-n parameter planes do the HSC models ever match the ratios measured from the sun, while they do match the FPCS ratios from Puppis. Thus we have no decisive X-ray evidence for relative abundance anomalies in Mg, Si, and S or in O, Ne, and Fe. While Puppis A may well have been a Type II supernova, as might be indicated by the oxygen rich optical knots, and produced 3 solar masses of oxygen and neon, it appears unlikely that the ejecta would be well mixed with the swept up ISM. On the contrary, as an ejecta shell is decelerated by the swept-up ISM, it will clump into tongues due to Rayleigh-Taylor instabilities (Gull 1975).

We would like to combine the information from all the separate diagnostics into a single model that can match all the measured X-ray spectra. Combining the indications from the FPCS and SSS diagnostic line ratios suggests that non-equilibrium models with current electron temperatures near 1 keV might be appropriate. In addition to matching the lines used as diagnostics, the models should reproduce the other features of the SSS spectra. With the column density fixed at 4×10^{21} equivalent hydrogen atoms cm^{-2} we fit all of the HSC models against our spectra. We allow each field to have different Sedov parameters to account for the obvious inhomogeneities of the remnant; however we assume only one component is present within each field. Although Puppis

is certainly not the ideal, spherically symmetric Sedov remnant, the imaging data supports the idea that the Sedov solution may hold locally, as Petre et al. (1982) found the emission at places on the rim to match that predicted from the limb of an adiabatic remnant in projection. Although the model spectra are calculated for the integrated emission from an entire remnant, the emission is so highly concentrated towards the boundary that spectra taken from smaller samples of the boundary should approximate those from the whole remnant models.

The model that gave the best fit for each of the fields is shown in Figure V.5. The quality of the fits may look poor in detail, but is actually surprisingly good considering that with n_H and all the abundances fixed, there were no parameters available to adjust the individual sections of the fit. No attempt was made to interpolate between the models that were calculated for a grid of discrete values of the Sedov parameters.

For each of the four spectra the parameters of the two models giving the best agreement is shown in Figure V.6. Only for field I does one of the models give a significantly better fit, labelled I1 in the figure. The labels "e" and "n" indicate whether or not (respectively) the electron temperature is assumed to equilibrate with the kinetic temperature of the ions at the shock. These SSS spectra do not discriminate well between the two extremes, as the major effect is upon the shape of the high energy continua. As long as the plasma is still ionizing and the electron temperature is greater than the current

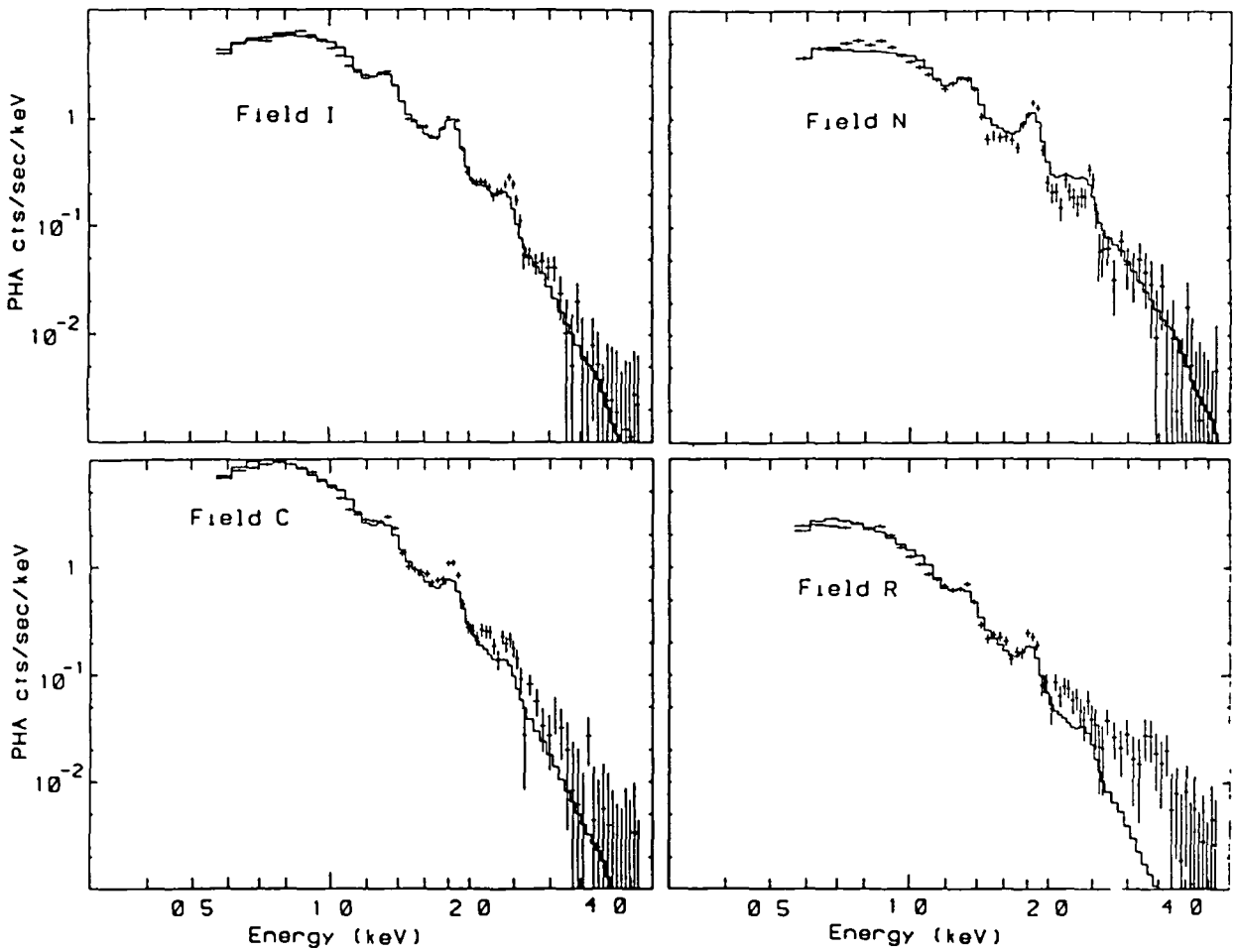

Figure V.5: The spectra are shown with the best fit model folded through the detector response.

ionization temperature, the lines are not affected much by the value of that temperature. The ionization rates are proportional to $T^{1/2}$, so the lines from the higher ion stages will occur sooner in the models with equilibration, but once those models get delayed trying to pass the two-electron state, the slower models, without equilibration can catch up.

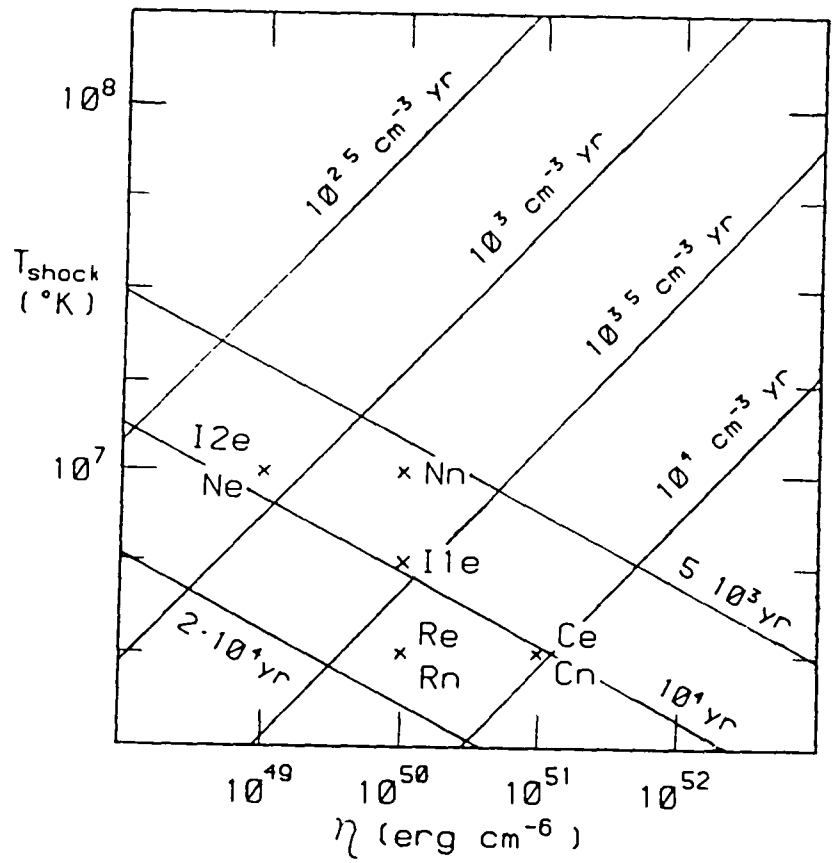

Figure V.6: Best fit model parameters placed on T_{shock}-n parameter plane. See text for details.

As expected from their relative excess of soft counts, fields C and R prefer lower shock temperatures than fields I and N. From the high resolution image Petre et al. (1982) concluded that the shock had hit a cloud in region C. The shock velocity would be slower in the increased density of the cloud and the post-shock temperature would be lower by the ratio of the density contrast. It is possible that spectrum R is dominated by emission from other density enhancements that the shock has encountered. Region R2 shows no obvious features in figure V.1 but contributes little to the combined spectrum. Region R1 includes a small bright spot. Region R3, which supplies most of the counts in spectrum R, shows a small inward curvature of the X-ray boundary similar to that

seen in field C, which Petre interpreted to be due to the shock being impeded by the larger density.

The solid traces in Figure V.6 are lines of constant age and are labelled with values of t x $E_{51}^{-1/2}$ in years ($E_{51} \equiv E/10^{51}$ ergs). The parameters of the fits cluster in a small region near the line for 10^4 years. This indicates a welcome consistency with the model explaining the different spectra as arising from one shock encountering different densities in the different regions.

The emission from a region may correspond to a slightly younger model if that emission is dominated by a recently encountered density enhancement, as is suggested for field C. If density inhomogeneities are the rule, as is suggested by the image, the emission, particularly in the brighter areas where clouds are most likely to have been swept up, may generally be younger than the age indicated by the size of the remnant.

The parameters of these models give reasonable values for the densities and inferred radius of the remnant. These models correspond to densities ~1.0 cm^{-3} for field C, ~0.3 cm^{-3} for field R and one model of fields I and N, and ~0.1 cm^{-3} for the other models for field I and N. Remnants of age $t \simeq 10^4$ years would have radii of 10-20 pc at these densities. Puppis presents a projected radius of ~20 arcmins which corresponds to distances of 1.7-3.4 kpc. Thus from our spectra and the angular size we would assign Puppis A a distance ~2.5 kpc, which is consistent with previous determinations (eg. ~2.4 kpc, Caswell and Lerche 1979).

The above calculations are for the case where the entire life of the shock was spent in the model density. In the case where the shock recently entered a region of increased density, there will be no simple relation of T_{shock} and $n_0 t$ with radius. The radius can be much larger than is implied by the current shock temperature.

As an approximate consistency check, we can compare our model pre-shock densities of 0.1-1 cm^{-3} with our measured surface brightness, which is independent of distance. Inverting the surface brightness of field I, 9.6×10^3 phots cm^{-2} $ster^{-1}$, using the emissivity of the best-fit non-equilibrium model, gives $n \simeq 0.46\ (fl)^{1/2}$, where f is the filling factor, and l is the thickness of the emitting region in parsecs. The thickness of ~3 parsecs, required to match a post-shock density four times larger than the model pre-shock density for this field, would be about 15% of the radius at the distance of 2.5 kpc. This is a reasonable thickness for the emitting shell.

Conclusions

The SSS obtained spectra from various positions within the Puppis A remnant and there were significant differences between some of the spectra. A number of observational and theoretical grounds suggest the use of realistic models that consider time-dependent ionization rather than multiple component equilibrium models with arbitrary abundances. We found non-equilibrium models using cosmic abundances could give reasonable approximations to the observed spectra. Other X-ray measurements, which had been interpreted as requiring an enrichment in Puppis A similar to that predicted for a Type II supernova, were shown

to be consistent with our model without enrichment. In this scenario, the variations in the spectra arise from variations in the density that the shock is traversing in the different regions. With these X-ray spectra we have shown that the ISM around Puppis A is inhomogeneous, with density contrasts of ~10, and does not differ much in composition from the material that is found around us.

VI. SPECTRA OF TWO YOUNG REMNANTS

Introduction

While old remnants, like Puppis A, are dominated by material from the ISM, young remnants should be able to supply more information about the supernova progenitors. The SSS observed five remnants of supernovae that occurred during historical times. Here we briefly mention the three we will not address in this work, and give reasons why they differ from the two we will investigate. The X-ray emission from the remnant of the supernova of 1054 AD, the famous Crab nebula, arises largely from nonthermal processes due to the pulsar. Cas A, which shows strong lines in the SSS observations (Becker et al. 1979), has an extremely complicated structure and history. There is no reliable age for Cas A as there is no report of a sighting of a corresponding optical outburst, which should have been visible. The optical remnant is quite complex, showing some slow moving clouds of emission and separate fast moving knots with large variations in inferred elemental abundances from knot to knot. The nature and quantity of this debris suggest that Cas A resulted from the explosion of a massive star, which is also suggested by the X-ray evidence for the presence of an expanding ring (Markert et al. 1983). The remnant of the supernova of 1006 AD shows a featureless X-ray spectrum (Becker et al. 1980), similar to that of the Crab nebula, which might also be due to nonthermal processes. Alternatively, it is possible that such a spectrum could arise in an extreme case of a nonequilibrium model similar to those we discuss below for SN1572 and SN1604 (Hamilton 1983). We leave further inspection of the SSS data from these three remnants for another work.

Now we turn to a re-examination of the SSS spectra from the remaining two remnants. Observations of the supernovae of 1572 and 1604 were recorded, principally by Tycho Brahe and Johannes Kepler (respectively). The positions of these outbursts were recorded in enough detail so that there can be little question that the modern optical, radio, and X-ray remnants came from these explosions. From the recorded descriptions of their apparent brightnesses Baade (1943, 1945) was able to construct estimates of the optical light curves. The light curves from both outbursts are consistent with the characteristic shape of the light curves of Type I supernovae. Assignment of supernova type is based upon optical spectra and light curve shape cannot be used for a definite classification. Occasionally a spectroscopic Type II will mimic the Type I light curve. Nevertheless, both the remnants are widely considered to have resulted from Type I supernovae. Even though we cannot be absolutely certain that these supernovae were of the same type, the explosions provided remnants of known ages which are not too distant or obscured for reasonable examination.

The now conventional model for a Type I supernova, reviewed in Chapter II, suggests that the particular shape of the optical light curve arises from the radioactive decay of ^{56}Ni produced in the explosion. The optical magnitude suggests that several tenths of a solar mass of nickel decays first into ^{56}Co and then into ^{56}Fe. If this large quantity of iron is heated with the rest of the remnant, it would show prominently in the X-ray spectra, so these spectra might provide a observational test of the nickel decay models.

Previous Observations

The remnant of Tycho's supernova has been relatively well observed at all conventional wavelengths. In the radio, the remnant appears as a limb-brightened shell, which when examined at high resolution can be separated into several circular arcs with slightly different radii, and at least one section where the limb appears straight (Henbest 1980). Faint optical filaments are present in the radio shell to the north and east (Minkowski 1959, Kamper and van den Bergh 1978). Spectroscopy of these filaments shows only lines of hydrogen. The line profiles have a narrow core surrounded by a much broader line. Such profiles could be produced by charge exchange from a shock of velocity ~2300 km/sec (Chevalier, Kirshner and Raymond 1980).

The expansion of the remnant has been followed in the optical (Kamper and van den Bergh 1978) and in the radio (Strom, Goss, and Shaver 1982). Except at the position of the optical filaments in the east, where velocities may be lower due to an encounter with denser material, the bulk of the remnant appears to be expanding at ~0.26 arc sec/year. This value corresponds to a dimensionless expansion rate, vt/r, of 0.47, which is larger than 0.40, the value for a Sedov remnant.

Determination of the distance to the remnant is, as is usual, quite difficult. From rather similar H I absorption spectra, Albinson and Gull (1982) infer a distance in the range 2-2.5 kpc, while Schwarz, Arnal and Goss (1980) obtain 4-5 kpc. Combining the observed proper motion of the optical filaments with the shock velocity derived from the line profile model, Chevalier, Kirshner, and Raymond (1980) derive a distance of 2.3±0.5 kpc, and argue that the high distance estimates

require average expansion velocities larger than the commonly held initial ejecta velocities of ~10,000 km/sec.

Tycho's remnant has been well studied by the various generations of X-ray detectors. Proportional counter observations of the X-ray spectrum of the remnant of Tycho's supernova show lines due to iron, silicon, and sulfur superposed on a continuum which required at least two thermal components (Hill, Burginyon, and Seward 1975; Davison, Culhane, and Mitchell 1976; Pravdo et al. 1980). The details of the analysis of the high resolution image by Seward, Gorenstein and Tucker (1983; hereafter SGT) will be placed into the discussion where they affect the modelling.

As the remnant of Kepler's supernova is a southern hemisphere object located in a crowded field near the galactic center, it has not been observed as well as Tycho's remnant. After examination of the descriptions of the outburst of Nova Ophiuchi of 1604 convinced Baade (1943) that it had been a supernova, he searched optical plates and found a faint fan-shaped nebulosity. Spectra of this nebulosity (Minkowski 1943, van den Bergh et al. 1973, van den Bergh 1980) are similar to those of the Crab nebula with relatively bright [N II] lines; and also similar to those of N49 in the Large Magellanic Cloud in that both show large number of [Fe II] emission features. The proper motions of the optical remnant indicate that it is "moving" northward while expanding slowly (van den Bergh and Kamper 1977). Over time a few of the flocculi have brightened, but none have been seen to fade. The optical appearance and dynamics of these flocculi are similar to that of the quasi-stationary flocculi in Cas A, which are believed to be pieces

of envelope material that had been ejected before the supernova, and were subsequently accelerated and compressed by the supernova shock. This gives Kepler's remnant an optical appearance much different than Tycho's, but in both cases the optical emission comes from the small amount of material in dense condensations and is not representative of the bulk of the remnant.

At 5 Ghz, the radio remnant of Kepler's supernova appears as an incomplete shell, with the brightest "clumps" of emission strung along the north, including one in the north-west at a position corresponding to the largest patch of optical nebulosity (Gull 1975a). Measured with a beam with a diameter about half that of the remnant, the polarization at 2700 Mhz is only 1-2% of the total power intensity (Milne and Dickel 1974).

Due to the proximity of the galactic center sources, the X-ray counterpart was not found until 1978 (Tuohy et al. 1979, Bunner 1979). The images taken with the instruments of the Einstein Observatory show an incomplete shell with bright regions approximately correlated with the radio map and a maximum near the largest optical nebulosity (White and Long 1983). As the remnant is neither as large or bright, these images cannot show the types of internal structures that are present in the image of Tycho's remnant.

SSS Observations

SSS spectra of both these remnants have been presented previously (Becker et al. 1980a, Becker et al. 1980b). Late in the mission, ~3000 seconds of data were taken at each of two additional positions in

Tycho's remnant. These positions are shown superposed on the contour diagram of SGT in Figure VI.1. No significant differences were found

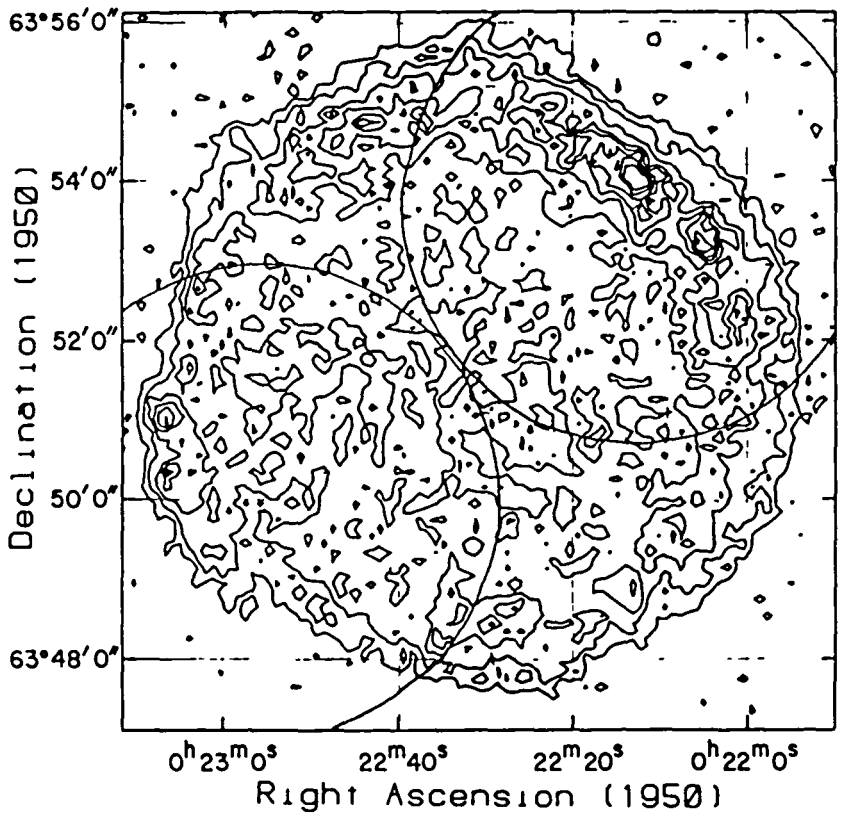

Figure VI.1: The positions of the SSS field of view for the observations of Tycho's supernova remnant that produced the spectrum used here, shown on the HRI contour map of Seward, Gorenstein, and Tucker (1983).

between the spectra taken at the two positions and they were added together. This spectrum contains more information about the low energies than that published since it was obtained with a much smaller absorbing layer of ice on the front of the detector. After the analyses were performed for those first papers, the calibration of the detector was extended to lower channels so we present here spectra for both

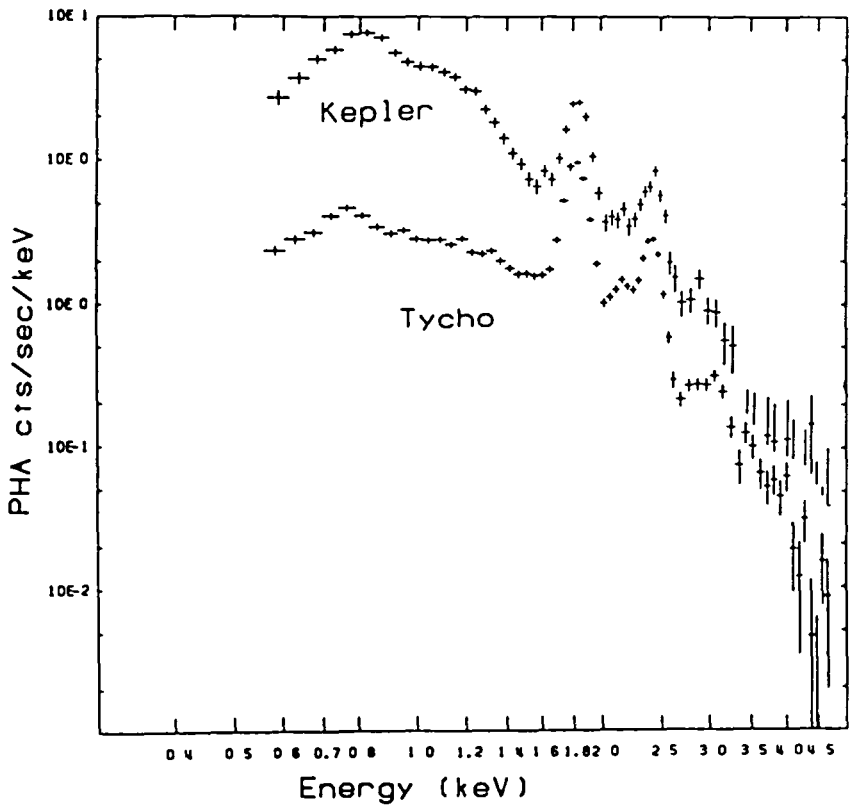

Figure VI.2: The SSS pulse height spectra for the remnants of Tycho's (lower) and Kepler's (upper) supernovae, corrected for the absorption due to the layer of material on the detector.

remnants down to lower energies. Figure VI.2 presents the PHA spectra for both remnants, corrected for the difference in the ice thickness. The lines appear similar, although the spectrum from the Kepler remnant shows a large excess at low energies not seen in the Tycho remnant.

Realistic Models of Young Remnants of Type I Supernovae

Early models for these particular young remnants suggested total masses much larger than the amounts thought to be ejected in a Type I supernova. This implied that the amount of swept up material was sufficiently high so that the remnants had definitely entered the Sedov

phase. More recently, estimates of some of the parameters have tended to change in the directions that reduce the estimates of the emitting mass, so we must re-examine the assumption that these remnants have progressed to the adiabatic phase. The estimates of the distances have tended to decrease, so that the inferred emission volume and densities have decreased. There is growing acceptance for large fractions of the volume of the ISM having densities lower than was considered common, and as the density estimates decrease, so do the estimates of the amount of material swept from the volume of the remnant. Several new considerations have decreased the mass of material required to produce the measure X-ray fluxes. First, the smaller distance estimates lower the luminosity corresponding to a given flux. Second, nonequilibrium effects can increase the plasma emissivity, particularly for low energy X-rays, so that the luminosity produced by a given mass of plasma is larger than predicted for that same mass in equilibrium. Lastly, the emissivity per electron can be greatly increased in a plasma enriched in heavy elements, as would be expected for supernova ejecta (Long, Dopita and Tuohy 1982).

In addition to the above arguments that these remnants may not have yet entered the Sedov phase, there is more direct evidence that more elaborate models are required. The expansion rate, measured in the optical and radio, is larger than is predicted for a Sedov phase remnant. While there are other models that could explain the faster expansion, such as adiabatic phase expansion modified by the evaporation of clouds in the interior of the remnant (Chieze and Lazareff 1981), larger rates of expansion may indicate that the remnant is still in the earlier phase.

The analysis of the HRI image by SGT directly shows that Tycho's remnant has a more complicated structure than that of an adiabatic remnant. In the image, an outer "shelf" of emission is identified as coming from the blastwave. The many irregular, patchy "clumps" of emission distributed in the limb-brightened "shell" are identified as supernova ejecta. In addition to the separately discernible clumps there is a diffuse emission in the same spherical shell with the clumps, identified as more supernova ejecta. Some 72% of the HRI counts arise from regions identified as ejecta. Even when allowance is made for higher emissivities in the ejecta, this soft X-ray image indicates that the remnant has not yet swept up sufficient material to have entered the adiabatic phase.

Our line strength measurements also lend strong evidence towards a large percentage of the X-ray emission arising in hot ejecta rather than in ISM heated by a blastwave. The equivalent widths of the silicon and sulfur lines in these remnants are much larger than can be produced by any equilibrium, cosmic abundance plasma. Although the inclusion of time-dependent ionization can enhance the line strengths compared to the predictions for the equivalent remnant in equilibrium, this enhancement is never sufficient, as had been thought possible, to match the observed lines. Although the line strengths can be increased by factors of several hundred over those in the equilibrium models, the equivalent widths never approach those observed, even for the most extreme remnant parameters.

Most of the above arguments for why these remnants may be in the transition period between the free expansion and adiabatic phases

involved observational evidence from the remnant of Tycho's supernova. Although we do not have similar evidence to show that transition period models might also be appropriate for Kepler's remnant, there are several arguments that lead us to consider them. The remnant of Kepler's supernova is younger by 32 years, so if the explosion had similar energy and ejected mass and occurred in a region of similar density, it will be in a slightly less advanced state. The larger estimates of the distance to Kepler's remnant place it far out of the plane of the galaxy, where the density of a smoothly distributed ISM would be low. An explosion in a lower density expands faster, but sweeps up mass at a lower net rate, and will spend more time in the transition period. These remnants are both small enough so that they may still be expanding into a region where the density was determined by the pre-supernova evolution of the progenitor. The densities these remnants are encountering might then be more similar than their different heights in the galaxy would indicate, as the great uniformity of Type I supernovae could stem from uniform progenitor evolution that would set up similar conditions near each explosion.

Models for the X-ray emission during the transition phase depend upon the details of the density distribution of the pre-supernova star and upon the details of the explosion process. We cannot expect to explore the space spanned by all the allowed values of all the parameters describing these details and must find a simpler approach.

One approach to modelling the early phases of remnants is to conduct numerical experiments using hydrodynamic computer codes (Rosenberg and Scheuer 1973; Mansfield and Salpeter 1974; Gull 1973; Itoh 1977; Jones, Smith, and Straka 1981). Until the model remnant has converged into a phase for which a similarity solution exists, most of the results from one numerical model can only be extended to a single parameter family of explosions similar to the one calculated. Numerical modelling requires large computer resources, and cannot be used to search much of the multi-dimensional parameter space, although is still required to check the details of specific models.

Efforts have been made at making models for the early time evolution more tractable (Gaffet 1978). A recent advance for this modelling has been the discovery of families of similarity solutions for the free expansion and transition periods (Hamilton 1983, Chevalier 1982). These solutions apply as long as the density distribution in the surrounding material and in the ejecta are simple functions in radius. They have been calculated for a constant external density or for one which varies as r^{-2}, as might be established by a constant wind from the progenitor. Hamilton's models are for thin, uniformly expanding shells of ejecta. Chevalier's apply while the reverse shock is traversing an outer section of ejecta with a density distribution $\propto r^{-n}$; with n greater than 5. Of these models, two have been investigated in greater detail for application to supernovae. The first, ejecta with a steep ($n \approx 12$) density distribution expanding into a r^{-2} external density, is used to model the explosion of a massive star into material that the star shed in an earlier period of stellar wind. The second of these similarity solutions is that of ejecta with a r^{-7} fall off expanding into a uniform

circum-stellar medium. The outer layers of any n=3 polytrope, such as a massive white dwarf, tend toward this density distribution in most types of explosions (Colgate and McKee 1969). Chevalier (1981) showed that such a density distribution could match the observations of the early-time light curves, which are determined by the distribution of the opacity above the expanding photosphere. In his model explosion, the power law density distribution was established in the outer ~40% (by mass) of the ejecta. The form and stability of the analytical solution, which we adopt for this examination of these remnants, was verified numerically by Jones and Smith (1983).

A remnant that is in the transition period described by the Chevalier similarity solution will have two regions of X-ray emission, which can be modelled separately. Hamilton (1983a, 1983b) has shown that for both these regions there are Sedov models that have approximately the same distribution of ionization times with emission measure, and thus yield similar spectra. He gives prescriptions for relating the parameters of the similarity solutions to those of the corresponding Sedov models. We approximated the X-ray spectra that would be produced by transition phase remnants by summing pairs of spectra drawn from the models of non-equilibrium, adiabatic phase remnants calculated by Hamilton *et al.* (1983). Assuming equal molecular weights, the average temperature of the blastwave region will be ~2.4 times hotter than the ejecta which has been heated by the reverse shock. Due to the larger density, the ionization time, nt, of the hot ejecta is ~1.7 times greater than that of the blastwave material. The emission from the inner shock would only be about 30% of that of the outer shock if the same emissivities apply to material in both regions. The emissivity of the ejecta can be much

higher though, due to the enrichment of the heavy elements (Long, Dopita and Tuohy 1982), and the reverse shock region can dominate the low-energy X-ray spectra. In a highly enriched plasma, most of the electrons are still attached when the ions are near the shock and could not be heated by equilibration mechanisms that might function there (Hamilton 1983). We therefore can use for the inner shock component a Sedov model in which the electrons are heated relatively slowly by the infrequent Coulomb collisions, with the elemental abundances left free to vary, and with the overall normalization free to vary to account for the emissivity enhancement due to the large number of electrons present in a highly enriched plasma. For the blastwave component we use a Sedov model with a higher shock temperature and expect the elements to be present at their cosmic abundance. We try both the models where the electrons are assumed to immediately equilibrate with the ions, and those where they are heated more slowly, although observations of a component as hot as 20 keV (Pravdo and Smith 1979) in Tycho appear to indicate that at least some of the electrons are heated quickly. The expected emissivity enhancement due to the enrichment of the ejecta component is likely to cause emission from that component to dominate the flux in the SSS bandwidth. The blastwave component is included primarily to match the high energy spectra and the imaging data.

Before testing the models for overall fit, which is affected by continuum and adjustable strengths of unresolved lines, the large lines in the spectra of these remnants can be used for ionization state diagnostics.

The high energy data from Tycho's remnant (Pravdo et al. 1980) shows a Kα line complex from iron with centroid located at 6.62+0.05-0.07 keV (2σ) and equivalent width ~1.2keV. In an equilibrium plasma this line energy would correspond to a temperature in the range ~0.8-2.0 keV, while the measured equivalent width, which is about as large as possible for any equilibrium plasma with cosmic abundances, corresponds to a temperature ~3.4 keV. A non-equilibrium plasma allows larger equivalent widths, particularly in the models where the electrons are heated slowly, not because the lines are enhanced, but because the continua are lower. There is a possibility that the 6.7 keV iron lines, which must arise in material that is hotter and/or has a larger nt than may be allowed by the lower energy lines, comes primarily from the blastwave component.

The SSS spectra of both remnants show large Heα lines from silicon and sulfur, but require that any Lyα lines be less than one tenth as bright. In an equilibrium plasma such line ratios could only occur over a small range of temperatures, from ~0.3-0.5 keV. In a plasma which is still ionizing, these line ratios can occur for various spans of time for a larger range of post-shock temperatures. To estimate this range of times we conducted some numerical simulations of the ionization of silicon and sulfur. We followed the time-dependent ionization of each element after suddenly heating neutral atoms to various temperatures at constant density. The times at which the helium-like ions begin to form and the times at which the fraction of ions in the hydrogen-like stage reaches ten percent are shown in Figure VI.3. The region allowed by the line measurements is hatched. In a Sedov remnant enriched in silicon and sulfur, large equivalent width Heα lines can dominate over the Lyα

lines for more of the parameter space than the simple simulations might indicate, since the density drops after the material is shocked due to the expansion of the remnant.

Although the above arguments indicate which models we expect will apply to these remnants, we fit the data against all the models in order to find the best fit without imposing any pre-conceptions. To limit the

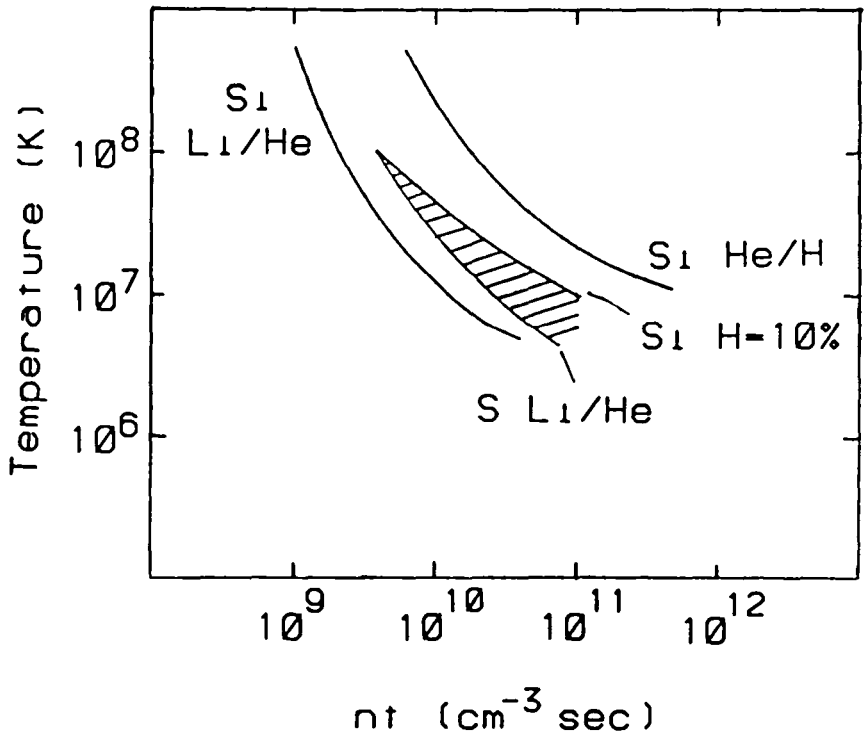

Figure VI.3: Results from the simulations showing when the two-electron states of Si and S start to form, and when the fraction in the one-electron state approaches 10%. The region allowed by our measurements is shown hatched.

computational demands, only one nonequilibrium component was used in the first fits of all the HSC models against the data from these two

remnants. We allowed the column density of absorbing material in the line of sight to vary freely in the absence of reliable information as to the values. Radio measurements of HI columns can only be used with caution: X-ray spectra of the Crab Nebula indicate column densities three times greater than the radio values. Most of the absorption comes from interstellar oxygen so the difference may come from a larger oxygen abundance in the line of sight than in the absorption models. Two narrow lines of arbitrary strength were included in the model to account for emission from argon, which was not included in the non-equilibrium models. The first of these was allowed to vary in energy slightly around 3.14 keV, the position of the Heα resonance transition, to account for the shifts in centroid due to di-electronic satellites and the Lyα lines. The second line energy was fixed at 3.702 keV, the energy of the Heβ transition. To set a point for the abundance determinations, the abundance of silicon versus hydrogen was fixed at 100 times solar. This decreases the emission from hydrogen and helium so that the dominant continuum is produced by heavy elements as would be the case for enriched ejecta. We then fit each of the available HSC models against the data, letting the program adjust the eleven model parameters. With so many free parameters there is a rather slow decrease in goodness of fit away from the best fit and we cannot claim that there is much reason to prefer any one of the best fitting models. Nevertheless, we present the best fitting models as representative of the class of acceptable models, though in reality we examine each of the top several models. The best fitting models are shown with the data in Figure VI.4; the parameters of these models are listed in Table VI.1.

We found that we can get good fits to these young remnants with Sedov models, with shock temperatures in the range of 3-6$\times 10^6$ K, and ionization times, nt, near 10^4 yr cm^{-3}. This may at first seem cool and old for such young remnants. The low temperatures could

Table VI.1: The parameters of the models giving the best fits. Both models had $\eta=10^{5\,1}$.

	SN 1572	SN 1604
T_{shock} (K)	$10^{6.75}$	$10^{6.5}$
Mg/Si	0.02	0.05
S/Si	2.1	2.4
Ca/Si	6.5	3.4
Fe/Si	0.08	0.33
n_H	7.4(21)	6.9(21)

be due to the slow rate at which electrons that are not free at the shock are subsequently heated. Large ionization times would arise in the high densities of clumps of ejecta formed due to Rayleigh-Taylor instabilities. With all the abundances free to vary, a wide range of models can adequately match the data, and we cannot place tight constraints on the values of the shock temperatures or ionization times. More interesting is the abundance information we can derive without requiring smaller ranges on the parameters.

While we have demonstrated that it is possible to find models that match our spectra, we must consider if the parameters are reasonable. For the fitting, the abundances of the elements in the ejecta component were left free to vary. Figure VI.5 presents the ratio of the fit

abundances to the silicon abundances, relative to the same ratio for cosmic abundances (i.e. $(X_i/X_{Si})_{ejecta}/(X_i/X_{Si})_{cosmic}$). These fit abundances confirm the impressions one gets from examining the spectra; little (if any) magnesium, large amounts of silicon and sulfur, and more

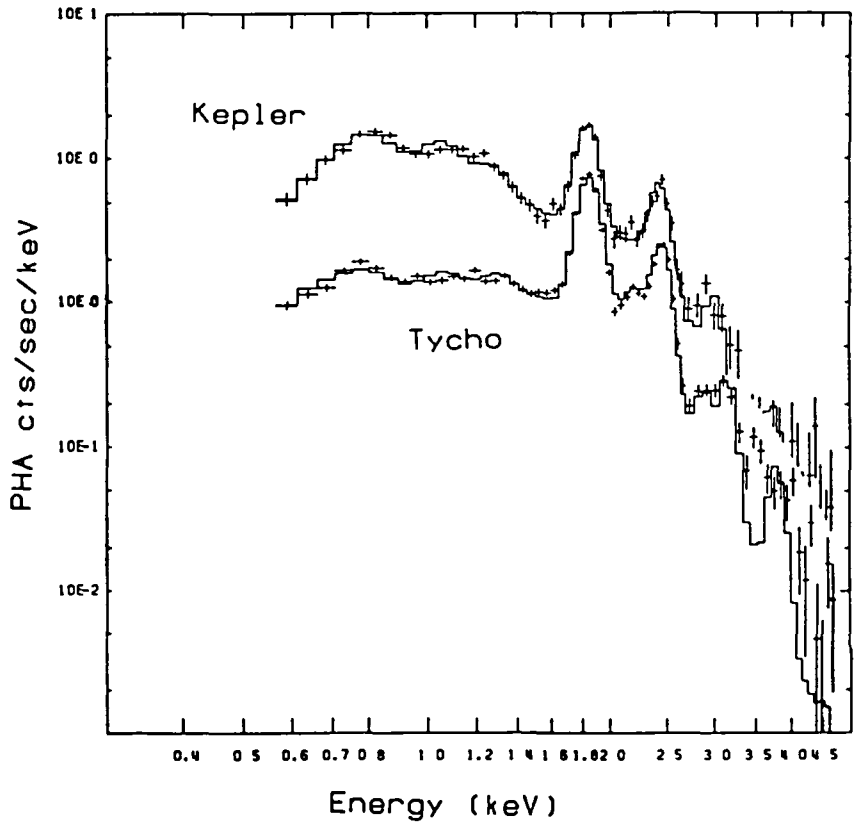

Figure VI.4: The pulse-height spectra that would be produced by the best fit models are shown with the data.

iron in Kepler than in Tycho. This substantial enrichment of the silicon group elements, which is also indicated by optical spectra from Type I supernovae during outburst, rules out helium detonation models that make only iron group elements. The quantitative values are quite similar to those predicted by Nomoto (1984) for the outer layers of the

ejecta from a carbon deflagration supernova. These nucleosynthesis predictions are shown on the figure.

The largest apparent discrepancy from the abundances predicted for

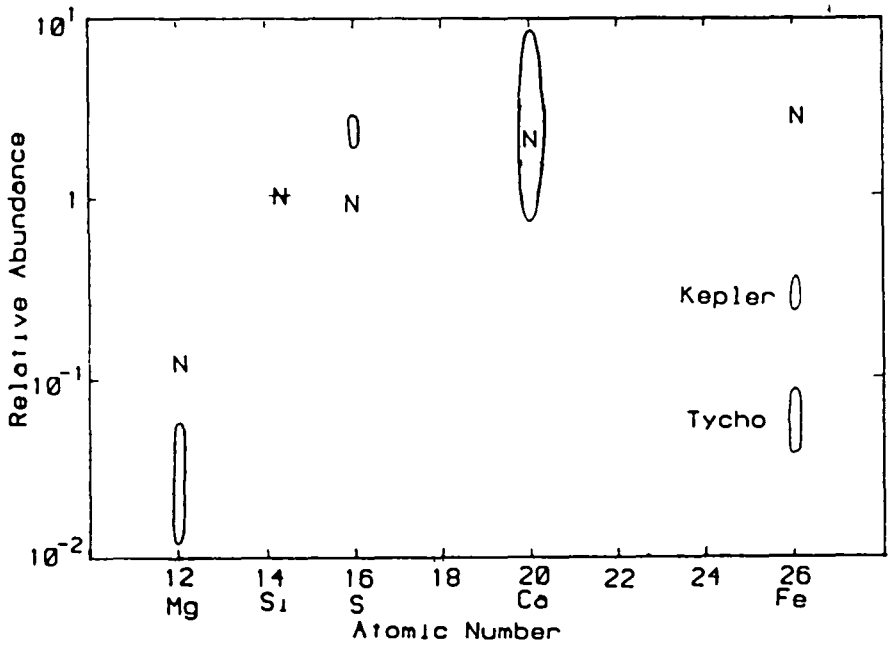

Figure VI.5: The ratio of elemental abundance relative to silicon from the model fits relative to the same ratio for cosmic abundances. The outlines give the envelope of the abundance values for the four best fitting values for each remnant. The points marked "N" are the nucleosynthetic predictions for a model of a carbon deflagration supernova by Nomoto (1984).

deflagration supernovae is for iron, which comes from the inner regions of the progenitor. These inner layers are ejected at lower velocities than the outer shells (Arnett 1980) and heated by the reverse shock only at late times. The lack of shocked iron in the ejecta is consistent

with our assumption that these remnants are still in the transition phase. Combining enhanced emission with a smaller distance gives a smaller total emitting mass and a smaller mass of swept up ISM, which is consistent with the smaller volume and lowered estimates of the ISM densities. In the transition phase, the appropriate similarity solutions predict that the mass processed by the reverse shock will be approximately equal to the swept mass. New, lower estimates of that swept mass correspond to masses of shocked ejecta small enough so that not much of the inner region of iron has been shocked long enough to have been ionized to the point of emitting X-rays. One indication that the iron is only recently shocked comes from the residuals from our fits between 0.7-1.1 keV. The excess of the data over the model at ~0.78 keV could well be due to emission from lower ionization stages of iron than are present in the "old" models. Figure VI.6 shows a model with the iron component from a model with nt ~10^3 yr cm^{-3} replacing the iron component of the previous best model. The increased abundance of iron in the models for Kepler may indicate that more of the iron core has been shocked, rather than that iron is more abundant. The depth that the reverse shock has penetrated into the ejecta is determined by the amount of swept material, which for remnants of approximately the same age, depends upon the ambient densities. One indication that the density around Kepler may be higher is the fact that the shock temperatures of the models that fit best tend to be lower than those of the models which fit Tycho's spectrum best. In the analysis of the imaging data, White and Long (1983) derived large densities for the emitting plasma. Thus even though Kepler's remnant is younger, it could well be in a more advanced state of evolution.

While this work was in progress, other groups investigated variants

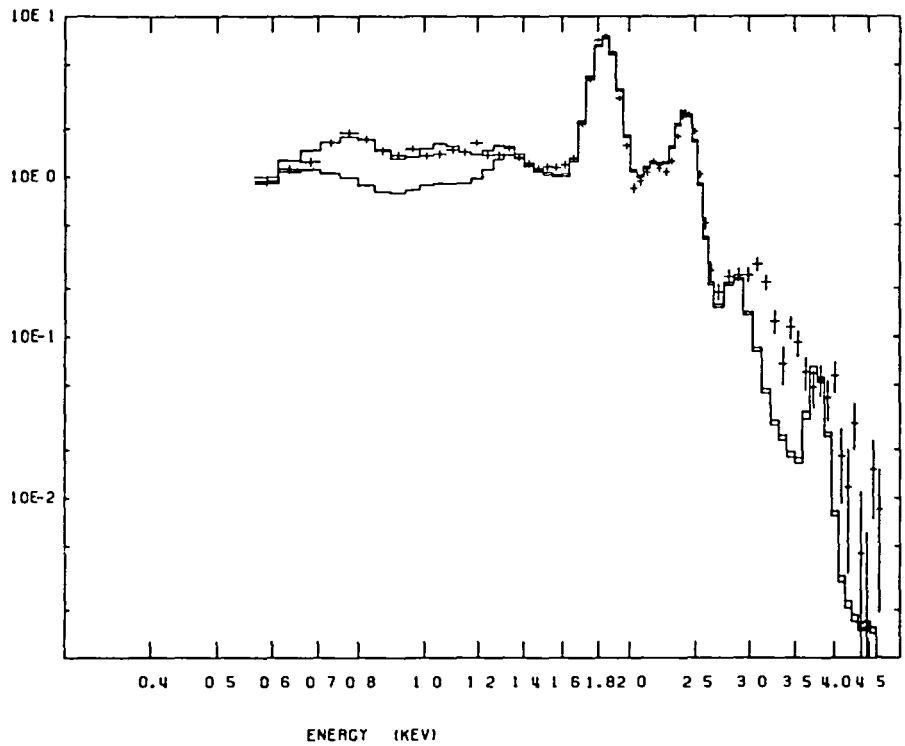

Figure VI.6: A "hybrid" model, with a younger iron component replacing the iron component of the best fitting models.

of the idea that some of the young remnants are in this transition phase. It has been proposed that the supernova of 1006 AD was a Type I (Minkowski 1966, van den Bergh 1976) and so the remnant might fit into some evolutionary sequence with these other suspected Type Is. Fabian, Stewart, and Brinkmann (1982) suggested that the lack of obvious lines in the X-ray spectrum of the remnant could be explained in a thermal model, with the interior of iron too cool to make lines surrounded by a shell of metal-poor material, perhaps swept from a wind. Wu et al. (1983) subsequently found apparent absorption lines due to cool iron in

the line of sight of a star believed to be behind the remnant. Hamilton (1983) developed a transition-phase model which explained the featureless spectrum as arising in an outer layer of pure carbon, with the heavier elements located in interior shells that have not yet been shocked up to X-ray temperatures. He then found that by allowing the shock to propagate further into ejecta with a similar layered structure, this model could reproduce the spectrum of Tycho's remnant. The difference in evolutionary state needed to produce the widely disparate spectra requires that the exterior densities only differ by a factor ~6.

The success of these first modelling attempts is encouraging; simple models for the early phases of the development of the remnants from Type I supernovae are able to reproduce the variety of spectra available thus far. Choosing among the various models and determining the values of the model parameters will probably require more observations and the consideration of all the detailed information present in imaging data.

Conclusions

Our X-ray spectra from the remnants of SN 1572 and SN 1604 show a similar pattern of intense lines from the silicon group elements. These line strengths cannot be matched by material with cosmic abundances under any reasonable conditions. The abundances required for agreement with models appropriate for emission from ejecta before the remnant has fully entered the adiabatic stage are qualitatively similar to those predicted for the outer layers of a carbon deflagration supernova. In our models the innermost layers of the star, predicted to be mostly

iron, have not yet been shocked or shocked for a long enough time to be emitting in the X-ray.

The principle difference between the two spectra is the greater emission from the L-shell lines of iron in the remnant of Kepler's supernova. This could be due to the reverse shock having advanced further into the ejecta due to a higher density around the remnant.

VII. FUTURE PROSPECTS

Work Remaining

This research suggests several types of investigations which can be pursued with other existing spectra of supernova remnants. Most all remnants with thermal spectra, except for remnants that are very old or have very high densities, are candidates for a non-equilibrium analysis. In order to have confidence in the ranges of abundances indicated by spectra requires that time-dependent ionization be considered in the absence of proof that equilibrium has been achieved. All the spectra from bright thermal remnants observed with the SSS should be re-examined with physically realistic models.

Unless it has collapsed into some compact remnant, the iron which powers the Type I light curve will be visible in remnants older than SN 1572 and SN 1604. It is possible that statistical accident has arranged there are no Type I remnants currently visible in the age range where large lines are produced from the iron, but we need to carefully examine the spectra from all the moderately old remnants to see if one might show tell-tale traces of its Type I legacy.

In addition to determining physical conditions and overall abundances, as done here, other remnants may have special conditions allowing other types of study. For instance, the remnant IC 443 may be interacting with a molecular cloud in the line of sight. In our spectra taken at various locations and in the data from the imaging instruments we appear to see varying amounts of obscuration.

If the ejection in some supernovae is asymmetric, as is suggested by the evidence for rings of emission in an increasing number of remnants, there will be abundance gradients in the remnants. While the existing spectra from remnants large enough for several fields of view probably do not have high enough quality for definitive statements, they should be examined for variations.

Although this work provides indications about some of the major questions in supernova and ISM research, most of them remain without definite answer. We have shown that the emission from the remnants of two young, suspected Type I supernovae is consistent with the abundances predicted for the outer layers of some popular models for such explosions. We have argued that the relative lack of emission from iron is not necessarily inconsistent with the inner region consisting of only iron group elements, as is also predicted by those models. While consistency with these models is encouraging, we cannot claim that we have proven that they accurately reflect the mechanism of these explosions. The presence (or absence) of large amounts of iron in the interiors of the young remnants will have to be determined at longer wavelengths where emission or absorption from cool iron that has not yet been shocked occurs. This would probably best be done with optical searchs for lines from low ionization stages. SN 1572 and SN 1604 do not appear to have any sources of featureless UV continua bright enough to be used for iron absorption studies with IUE.

Another area which requires more research is the efficiencies of the various mechanisms for heating the electrons. This will require a

combination of higher bandwidth, higher spatial resolution, and better calculations.

Further work on the spectra of remnants will require models that attempt to account for specific details of the inhomogeneities and structures present. While they could be used to map out the range of allowed models, the addition of these extra parameters does not seem justified by the currently available data.

Future Prospects

The existing observations demonstrate the utility of these types of spectrometers to the study of supernova remnants. Indeed, a major factor limiting the scientific return was the relatively short lifetime of the experiment. Although much more could have been learned given more time with the present instrument, there is great promise offered by reasonably modest extensions in instrument performance expected in the future.

In telescopes with greater area, observations to the same sensitivity can be performed faster, allowing more fields to be covered in a given time. Increases in the effective area improve the signal-to-background ratio and allows longer integrations and higher sensitivities. Improved shielding and background rejection techniques also improve the sensitivity and allow study of the great number of fields with lower surface brightnesses. Some of the new telescopes will have larger plate scales so that spectroscopy with better spatial resolution will be possible. Spectra that reveal the variations in the ionization states and temperatures with distance behind the shock, are needed to address

how and where the electrons are heated. By permitting searches for abundance inhomogeneities, spectroscopy with increased spatial resolution can be used to explore the layered structure of the progenitor and the evidence for asymmetric explosions. Increased plate scale can be a mixed blessing, as it decreases the sensitivity for surface brightness for a detector of fixed physical size.

The above performance improvements allow the types of studies that have been performed to be extended to smaller, dimmer fields. More exciting are the new capabilities that would come with increasing the energy range and spectral resolution without sacrificing the sensitivity and throughput advantages of non-dispersive spectrometers. Increasing the bandpass to higher energies would permit better constraints on the forms of the continua, important for determining the rate of heating in the plasma. More importantly, higher bandpass opens up new types of diagnostics possible with observations of the inner-shell lines of iron.

Due to its large relative abundance and high atomic number, iron provides strong lines which are well separated and not blended with lines from other elements. Lines from inner-shell transitions are excited at temperatures low compared to the ionization potential of the shell, so these diagnostics have greater range than might be apparent at first. The centroid of the Kα complex moves from 6.55 keV to 6.89 keV over temperatures ranging from 1-30 x 10^7 K. As a non-equilibrium diagnostic, this centroid can be used to measure how far the ionization has advanced on its way to higher ion stages. The Lyman α line in iron is far enough (267 eV) from the resonance line of the Heα triplet so that moderate resolution spectrometers can separate these transitions

which are blended in lower atomic number elements. The Lyα to Heα ratio is a diagnostic for how much of the iron has been ionized to the one-electron state, which is a high-temperature diagnostic for an equilibrium plasma or indicates how far time-dependent ionization has progressed.

Such capabilities would be realized by flying solid state spectrometers at the focus of the Broad Band X-Ray Telescope (BBXRT) or the Advanced X-ray Astrophysics Facility (AXAF). BBXRT, part of the OSS-2 shuttle payload, offers areas at 2 and 7 keV of 580 and 250 cm^2, with a spatial resolution ~1.6 arc minutes half power radius. The AXAF telescope, optimized for high (~0.5 arc second) spatial resolution, has areas at 2 and 7 keV of 1100 and 200 cm^2. In addition to opening up the bandpass at the high-energy end, improvements in solid state detectors and electronics will now allow spectra to be taken down to ~0.3 keV.

Other improvements in detector technology will allow instruments on these future missions to have much lower non-X-ray background and noise levels. Current technology detectors have spectral resolutions almost twice as good as the SSS on HEAO-2. A resolution of ~90 eV is sufficient to separate the Lyα line from the Heα line in elements down to neon. The ability to separate and measure more lines would allow much tighter constraints to be placed on plasma state.

Much higher spectral resolution may be possible in a new type of spectrometer now under study. The theoretical limit for these devices, which measure the amount of heat an X-ray deposits in a small element, can approach 1 eV. Such a non-dispersive spectrometer, mounted on AXAF, would supply a great advance for the study of thermal plasma. This

would allow the simultaneous observation of the individual lines of the Heα triplet from all the elements from neon through iron with nearly the entire area of the telescope. The constraints on plasma state and abundances that could come from spectra taken with such an instrument would help a great deal in the study of the nature of supernovae and the inter-stellar medium.

VIII. RECAPITULATION

We have examined the moderate resolution X-ray spectra from some of our observations of supernova remnants with models including time-dependent ionization. The differences between the spectra we obtained at different locations in the "middle-aged" remnant Puppis A can be approximately matched by a model shock propagating into different densities. In this model the densities vary by a factor of ~10 between our observed locations. This confirms the impression one obtains from the X-ray image that the medium around this remnant contains a range of density enhancements of various sizes.

Our models for Puppis A do not require any elements to be enhanced over their cosmic abundance. Any enrichment from the supernova ejecta could now be invisible in the X-ray, either because it has been diluted with the large amount of ISM the remnant has encompassed, or because the ejecta formed dense blobs which cooled quickly. In this scenario we find that the abundances of the elements around the Puppis supernova are similar to those determined locally.

The X-ray plasma in the young remnants of the SN 1572 and SN 1604 has elemental abundances much different than the local values. Our spectra have lines from the silicon group elements that are larger than can be produced under any reasonable conditions by material of standard composition. The large luminosities of these remnants required large emitting masses when standard emissivities were assumed. With enhanced emissivities, due to high metal enrichment of the plasma and non-equilibrium effects, the amount of mass required to produce the measured emission is sufficiently small so that the remnants can be in a

transition phase between the early free expansion stage and the adiabatic stage. In this phase, the reverse shock has not yet heated the innermost regions of the ejecta. Thus the fact that we do not observe emission from the large masses of iron predicted to be created by a Type I explosion need not rule out its presence.

For the material that is now heated, presumably the outer layers of the star, we obtain abundances that approximately agree with those calculated for a carbon-deflagration supernova (Nomoto 1984). In these types of models, the outer layers are burned past neon and magnesium into silicon group elements, and the inner region is burned to iron group elements. This is to be contrasted with other models, such as for carbon detonation supernovae, where only a small amount of material other than iron remains.

Although we find consistency with these first X-ray abundance determinations and some simple, commonly held theories, we must not consider this to indicate that the mysteries associated with the production of the elements have been solved. If the abundances in distant ISM are similar to those observed locally, a greater mystery is to explain why the composition is so similar, particularly considering that the local environment may have been modified by ejecta from a supernova that triggered the collapse of the proto-solar nebulae. Samples of distant material are brought to us as cosmic rays, and again, after allowing for the spallation and fragmentation that occurs along the way, the composition appears to be near solar. This is also surprising if cosmic rays are directly accelerated in the supernova explosions, as then the abundances should resemble those of enriched

ejecta. Although supernovae are the most obvious (and commonly held) sites for cosmic ray acceleration, they do not seem capable of producing the flux of ultra-high energy cosmic rays (>1 TeV) nor has the signature that a large population of lower energy particles in the remnant would give to the X-ray emission been observed. Supernovae have a major effect upon the dynamics and composition of the galaxy, but even more exotic mechanisms may be required to explain how it obtained its present state.

BIBLIOGRAPHY

Albinson, J. S., and Gull, S. F. 1982, Proc. Symposium Neutral Clouds near HII Regions, eds. R. S. Roger and P. E. Dewdney (Dordrecht: Reidel), p. 193.

Aldrovandi, S. M. V., and Pequignot, D., 1973, Astron. Ap. 25, 137-140, "Radiative and Dielectronic Recombination Coefficients for Complex Ions".

Arnett, W. D., 1980, Ap. J. 240, 105, "Nonuniform Abundances in Young Supernova Remnants".

Baade, W., 1943, Ap. J. 97, 119, "Nova Ophiuchi of 1604 as a Supernova".

Baade, W., 1945, Ap. J. 102, 309, "β Cas as a Supernova of Type I".

Baade, W. and Minkowski, R., 1954, Ap. J. 119, 206, "Identification of the Radio Sources in Cassiopeia, Cygnus A, and Puppis".

Becker, R. H., Holt, S. S., Smith, B. W., White, N. E., Boldt, E. A., Mushotzky, R. F., and Serlemitsos, P. J., 1979, Ap. J. (Letters) 234, L73-L76, "X-ray Spectrum of Cassiopeia A Measured with the Einstein SSS".

Becker, R. H., Holt, S. S., Smith, B. W., White, N. E., Boldt, E. A., Mushotzky, R. F., and Serlemitsos, P. J., 1980, Ap. J. (Letters) 235, L5-L8, "Elemental Abundances in a Type I Supernova Remnant".

Becker, R. H., Boldt, E. A., Holt, S. S., Serlemitsos, P. J., and White, N. E., 1980, Ap. J. (Letters) 237, L77-L79, "X-ray Spectrum of Kepler's Supernova Remnant".

Becker, R. H., Szymkowiak, A. E., Boldt, E. A., Holt, S. S., and Serlemitsos, P. J., 1980, Ap. J. (Letters) 240, L33-L35, "Is the Remnant of SN 1006 Crablike?".

Becker, R. H., and Szymkowiak, A. E., 1981, Ap. J. (Letters) 248, L23-L26, "High Resolution X-ray and Radio Images of the Crab-like Supernova Remnant G21.5-0.9".

Becker, R. H.,Helfand, D. J., and Szymkowiak, A. E., 1982, Ap. J. 255, 557-563, "An X-ray Study of two Crablike SNR: 3C58 and CTB 80".

Becker, R. H.,Helfand, D. J., and Szymkowiak, A. E., 1983, Ap. J. (Letters) 286, L93-L97, "G29.7-0.3: Another SNR with an Identity Crisis".

Bevington, P. R. 1969, Data Reduction and Error Analysis for the Physical Sciences, (New York: McGraw Hill).

Blisset, R. J. and Cruise, A. M., 1979, MNRAS 186, 45, "The Restoration of Astronomical X-ray Spectra".

Bodenheimer, P. and Woosley, S. E., 1983, Ap. J. 269, 281, "A Two-dimensional Supernova Model with Rotation and Nuclear Burning".

Brown, R. L., and Gould, R. J., 1970, Phys. Rev. D 1, 2252, "Interstellar Absorption of Cosmic X-rays".

Bunner, A. N., 1979, Bull. AAS 11, 461.

Cameron, A. G. W., and Truran, J. W., 1977, Icarus 30, 477, "The Supernova Trigger for the Formation of the Solar System".

Canizares, C. R. and Winkler, P. F., 1981, Ap. J. (Letters) 246, L33-L36, "Evidence for Elemental Enrichment of Puppis A by a Type II Supernova".

Canizares, C. R., Winkler, P. F., Markert, T. H., and Berg, C. 1983, in IAU Symposium 101, Supernova Remnants and Their X-ray Emission, eds. J. Danziger and P. Gorenstein (Dordrecht: Reidel), p. 205, "High Resolution X-ray Spectra of Supernova Remnants".

Caswell, J. L. and Lerche, I., 1979, MNRAS 187, 201-216, "Galactic Supernova Remnants: Dependence of Radio Brightness on Galactic Height and its Implications".

Chevalier, R. A., Kirshner, R. P. and Raymond, J. C., 1980, Ap. J. 235, 186-195, "The Optical Emission from a Fast Shock Wave with Application to Supernova Remnants".

Chevalier, R. A., 1981, Ap. J. 246, 267-277, "Exploding White Dwarf Models for Type I Supernovae".

Chevalier, R. A., 1982, Ap. J. 258, 790-797, "Similarity Solutions for the Interaction of Stellar Ejecta with an External Medium".

Chieze, J. P. and Lazereff, B., 1981, Astron. Ap. 95, 194-198, "Self Similar Evolution of Evaporative Supernova Remnants".

Colgate, S. and McKee, C., 1969, Ap. J. 157, 623, "Early Supernova Luminosity".

Cowie, L. L., McKee, C. F. and Ostriker, J. P., 1981, Ap. J. 247, 908-924, "Supernova Remnant Evolution in an Inhomogeneous Medium. I: Numerical Models".

Cox, D., and Tucker, W., 1969, Ap. J. 157, 1157, "Ionization Equilibrium and Radiative Cooling of a Low Density Plasma".

Davison, P. J. N., Culhane, J. L., and Mitchell, R. J., 1976, Ap. J. (Letters) 206, L37, "X-ray Spectra of Cassiopeia A and Tycho's Supernova Remnant Observed with Ariel 5".

Dopita, M. A., Mathewson, D. S., and Ford, V. L., 1977, Ap. J. 214, 179-188, "Optical Emission from Shock Waves. III: Abundances in Supernova Remnants".

Fabian, A. C., Stewart, G. C., and Brinkmann, W., 1982, Nature 295, 508, "Is the Remnant of SN1006 Composed of Iron?".

Fireman, E. L., 1974, Ap. J. 187, 57, "Interstellar Absorption of X-rays".

Gaffet, B., 1978, Ap. J. 225, 442-464, "Analytical Methods for the Hydrodynamical Evolution of Supernova Remnants".

Giacconi, R. et al., 1979, Ap. J. 230, 540-550, "THe EINSTEIN (HEAO-2) X-Ray Observatory".

Gorenstein, P., Harnden, F. R., and Tucker, W. H., 1974, Ap. J. 192, 661-676, "The X-ray Spectra of the Vela and Puppis Supernova Remnants and the Shockwave model of Supernova Remnants".

Green, A. J., 1971, Aust. J. Phys. 24, 773, "Radio Emission from the Supernova Remnant Puppis A".

Gronenschild, E. H. B. M., and Mewe, R., 1982, Astron. Ap. Suppl. 48, 305-321, "The Effects of Non-equilibrium Ionization on the X-ray Emission of Supernova Remnants".

Gull, S. F., 1973, MNRAS 161, 47-69, "A Numerical Model of the Structure and Evolution of Young Supernova Remnants".

Gull, S. F., 1975, MNRAS 171, 263-278, "The X-ray, Optical, and Radio Properties of Young Supernova Remnants".

Hamilton, A. J. S., Sarazin, C. L., and Chevalier, R. A., 1983, Ap. J. Suppl. 51, 115-148, "X-ray Line Emission from Supernova Remnants. I. Models for Adiabatic Remnants".

Hamilton, A. J. S., and Sarazin, C. L. 1983 in IAU Symposium 101, Supernova Remnants and Their X-ray Emission, eds. J. Danziger and P. Gorenstein (Dordrecht: Reidel), p. 113, "The Effect of SNR Structure on Non-equilibrium X-ray Spectra".

Hamilton, A. J. S. 1983, Ph. D. Thesis, University of Virgina.

Heiles, C., 1964, Ap. J. 140, 470, "Supernova Shells and Galactic X-rays".

Helfand, D. J. 1983 in IAU Symposium 101, Supernova Remnants and Their X-ray Emission, eds. J. Danziger and P. Gorenstein (Dordrecht: Reidel), p. 471, "X-rays from Radio Pulsars: The Portable Supernova Remnants".

Henbest, S. N., 1980, MNRAS 190, 833-851, "The Structure of Tycho's Supernova Remnant".

Hill, R. W., Burginyon, G. A., and Seward, F. D., 1975, Ap. J. 200, 158, "The Soft X-ray Spectra of Cassiopeia A and Tycho's Supernova Remnant".

Hillebrandt, W. 1982 in Supernovae: A Survey of Current Research, eds. M. J. Rees and R. J. Stoneham (Dordrecht: Reidel), p. 123, "Computer Simulations of Stellar Collapse and Supernovae Explosions: Non-rotating and Rotating Models".

Holt, S. S., 1976, Space Sci. Instr. 2, 205, "Si(Li) X-ray Astronomical Spectroscopy".

Itoh, H., 1977, P. A. S. J. 29, 813, "Theoretical Spectra of the Thermal X-rays from Young Supernova Remnants".

Itoh, H., 1978, P. A. S. J. 30, 489, "Two-Fluid Blast-wave Model for Supernova Remnants".

Itoh, H., 1979, P. A. S. J. 31, 541, "Theoretical X-ray Spectra of Supernova Remnants in the Adiabatic Phase".

Itoh, H., 1979, Nature 281, 656, "X-ray and [Fe XIV] 5303 Å Emission from Puppis A Supernova Remnant".

Jones, E. M., Smith, B. W., and Straka, W. C., 1981, Ap. J. 249, 185-194, "Formation of Supernova Remnants: The Pre-Blast-Wave Phase".

Jones, E. M., and Smith, B. W., 1983 in IAU Symposium 101, Supernova Remnants and Their X-ray Emission, eds. J. Danziger and P. Gorenstein (Dordrecht: Reidel), p. 83, "Very High Resolution Calculations of Very Young Supernova Remnants".

Joyce, R. M., Becker, R. H., Birsa, F. B., Holt, S. S., and Noordzy, M. P., 1978, IEEE Trans. Nuc. Sci. NS-25, No 1, 453-458, "The GSFC Solid State Spectrometer for the HEAO-B Mission".

Kahn, S. M., and Blisset, R. J., 1980, Ap. J. 238, 417, "The Direct Deconvolution of X-ray Spectra".

Kamper, K. W. and van den Bergh, S., 1978, Ap. J. 224, 851-856, "Expansion of the Optical Remnant of Tycho's Supernova".

Lampton, M., Margon, B., and Bowyer, S., 1976, Ap. J. 208, 177-190, "Parameter Estimation in X-ray Astronomy".

Lasker, B. M., 1978, Ap. J. 223, 109-121, "Studies of N132D, a Supernova Remnant similar to Cassiopeia A in the Large Magellanic Cloud".

Long, K. S., Dopita, M. A., and Tuohy, I. R., 1982, Ap. J. 260, 202, "The Effects of Ejecta on the X-ray Luminosities of Supernova Remnants".

Lotz, W., 1967, J. Opt. Soc. Am. 57, 873, "Ionization Potentials of Atoms and Ions from Hydrogen to Zinc".

Lucke, R. L., Zarnecki, J. C., Woodgate, B. E., Culhane, J. L., and Sooker, D. G., 1979, Ap. J. 228, 763-770, "[Fe X] and [Fe XIV] Emission from Puppis A and other Supernova Remnants".

Mansfield, V. N., and Salpeter, E. E., 1974, Ap. J. 190, 305-313, "Numerical Models for Supernova Remnants".

Markert, T. H., Canizares, C. R., Clark, G. W., and Winkler, P. F., 1983, Ap. J. 268, 134-144, "High Velocity, Asymmetric Doppler Shifts of the X-ray Emission Lines of Cassiopeia A".

Marquardt, D. W., 1963, J. Soc. Ind. Appl. Math. 11 No 2, 431-441, "An Algorithm for Least-Squares Estimation of Nonlinear Parameters".

McKee, C. F., 1974, Ap. J. 188, 335-339, "X-ray Emission from an Inward Propagating Shock in Young Supernova Remnants".

McKee, C. F., and Ostriker, J. P., 1977, Ap. J. 218, 148-169, "A Theory of the ISM: Three Components Regulated by Supernova Explosions in an Inhomogeneous Substrate".

Mewe, R., 1972, Solar Phys. 22, 459, "Calculated Solar X-radiation from 1 to 60 Å".

Mills, B. Y. 1983 in IAU Symposium 101, Supernova Remnants and Their X-ray Emission, eds. J. Danziger and P. Gorenstein (Dordrecht: Reidel), p. 551, "The Radio Properties of SNRs in the Magellanic Clouds".

Milne, D. K., 1971, Aust. J. Phys. 24, 429, "Radio Observations of the Supernova Remnants IC443 and Puppis A".

Milne, D. K., and Dickel, J. R., 1974, Aust. J. Phys. 27, 549-562, "2700 MHz Polarization Observations of 17 Supernova Remnants".

Milne, D. K., Goss, W. M., and Danziger, I. J., 1983, MNRAS 204, 237-239, "Radio Observations of the Supernova Remnant Puppis A".

Minkowski, R., 1943, Ap. J. 97, 128, "The Spectrum of the Nebulosity near Kepler's Nova of 1604".

Minkowski, R. 1959, IAU Symposium 9: Paris Symposium on Radio Astronomy, ed. R. N. Bracewell (Stanford University Press), p. 315.

Minkowski, R., 1966, Astr. J. 71, 371, "Supernova of +1006".

Nomoto, K. 1984 in Proceeding of Third Workshop on Stellar Nucleosynthesis, held in Erice, Italy, 11-21 May 1983, eds. C. Chiosi and A. Renzini (Dordrecht: Reidel), "Nucleosynthesis in Type I Supernova: Carbon Deflagration and Helium Detonation Models".

Nugent, J. J., Jr. 1983, Ph. D. Thesis, California Institute of Technology

Ostriker, J. P. 1982 in Supernovae: A Survey of Current Research, eds. M. J. Rees and R. J. Stoneham (Dordrecht: Reidel), p. 565, "Supernovae and the Formation of Galaxies".

Petre, R., Canizares, C. R., Kriss, G. A., and Winkler, P. F., 1982, Ap. J. 258, 22, "A High-Resolution X-ray Image of Puppis A: Inhomogeneities in the Interstellar Medium".

Pradhan, A. K., 1982, Ap. J. 263, 477-482, "On the Systematics of Line Ratios along the Helium Isoelectronic Sequence".

Pravdo, S. H., and Smith, B. W., 1979, Ap. J. (Letters) 234, L195-L198, "X-ray Evidence for Electron-Ion Equilibrium and Ionization Nonequilibrium in Young Supernova Remnants".

Pravdo, S. H., Smith, B. W., Charles, P. A., and Tuohy, I. R., 1980, Ap. J. (Letters) 235, L9-L12, "X-ray Line Emission from the Tycho Supernova Remnant".

Raymond, J. C., 1978, Ap. J. 222, 1114, "On Dielectronic Recombination and Resonances in Excitation Cross Sections".

Reynolds, S. P., and Chevalier, R. A., 1981, Ap. J. 245, 912-919, "Nonthermal Radiation from Supernova Remnants in the Adiabatic Stage of Evolution".

Rosenberg, I., and Scheuer, P. A. G., 1973, MNRAS 161, 27-45, "A Numerical Computation of the Dynamical Evolution of a Supernova Remnant".

Schwarz, U. J., Arnal, E. M., and Goss, W. M., 1980, MNRAS 192, 67P-71P, "The Distance to Tycho's Supernova Remnant (3C10) - a Rediscussion".

Seward, F. D., Gorenstein, P., and Tucker, W., 1983, Ap. J. 266, 287, "The Mass of Tycho's Supernova Remnant as Determined from a High Resolution X-ray Map".

Shklovsky, I. S. 1962, Soviet Astr. J., 6, 162 (translation of Astr. Zh., 39, 209).

Shklovsky, I. S. 1968, Supernovae, (London: Wiley-Interscience).

Shull, J. M., 1982, Ap. J. 262, 308, "X-ray Emission from Young Supernova Remnants: Nonionization Equilibrium Abundances and Emissivities".

Smith, B. W., 1977, Ap. J. 211, 404-420, "Hot Interstellar Tunnels. I. Simulation of Interacting Supernova Remnants".

Solinger, A., Rappaport, S., and Buff, J., 1975, Ap. J. 201, 381-386, "Isothermal Blastwave Model of Supernova Remnants".

Spitzer, L., Jr. 1962, Physics of Fully Ionized Gases (New York: Interscience).

Spitzer, L., Jr. 1978, Physical Processes in the Interstellar Medium (New York: Interscience).

Taylor, G. 1950, Proc. Roy. Soc. Lon. A201, 159-174, "The Formation of a Blastwave by a Very Intense Explosion. I. Theoretical Discussion".

Tidman, D. A., and Krall, N. A. 1971, Shock Waves in Collisionless Plasmas, (New York: Interscience).

Tinsley, B. M., 1979, Ap. J. 229, 1046-1056, "Stellar Lifetimes and Abundance Ratios in Chemical Evolution".

Trimble, V., 1982, Rev. Mod. Phys. 54, 1183-1224, "Supernovae. Part I: the events".

Trimble, V., 1983, Rev. Mod. Phys. 55, 511-563, "Supernovae. Part II: the aftermath".

Tsurutani, B. T., and Rodriguez, P., 1981, J. Geophys. Res. 86, 4319-4324, "Upstream Waves and Particles: An Overview of ISEE Results".

Tuohy, I. R., Nugent, J. J., Garmire, G. P., and Clark, D. H., 1979, Nature 279, 139-140, "Evidence for X-ray Emission from Kepler's Supernova Remnant".

Tuohy, I. R., Clark, D. H., and Burton, W. M., 1982, Ap. J. (Letters) 260, L65-L68, "The Peculiar X-ray Morphology of the Supernova Remnant G292.0+1.8: Evidence for an Asymmetric Supernova Explosion".

van den Bergh, S., Marscher, A. P., and Terzian, Y., 1973, Ap. J. Suppl. 26, 19, "An Optical Atlas of Galactic Supernova Remnants".

van den Bergh, S., 1976, Ap. J. (Letters) 208, L17, "The Optical Remnant of the Lupus Supernova of 1006".

van den Bergh, S., and Kamper, K. W., 1977, Ap. J. 218, 617-632, "The Remnant of Kepler's Supernova".

van den Bergh, S., 1980, Astron. Ap. 86, 155, "The Spectrum Of Kepler's Supernova of 1604".

Walker, A. B. C., Jr., Rugge, H. R., and Weiss K., 1974, Ap. J. 192, 169, "Relative Coronal Abundances Derived from X-ray Observations. II. Nitrogen, Oxygen, Neon, Magnesium, and Iron".

White, R. L., and Long, K. S., 1983, Ap. J. 264, 196-205, "The X-ray Surface Brightness of Kepler's Supernova Remnant".

Winkler, P. F., Canizares, C. R., Clark, G. W., Markert, T. H., and Petre, R., 1981, Ap. J. 245, 574-580, "X-ray Line Emission from the Puppis A Supernova Remnant: Oxygen Lines".

Winkler, P. F., Canizares, C. R., Clark, G. W., Markert, T. H., Kalata, K., and Schnopper, H. W., 1981, Ap. J. (Letters) 246, L27-L31, "A Survey of X-ray Line Emission from the Puppis A Supernova Remnant".

Woosley, S. E., and Weaver, T. A. 1983 in Essays in Nuclear Astrophysics, eds. C. Barnes, D. Clayton, and D. Schramm, (Cambridge, Cambridge University Press).

Woltjer, L. 1970, IAU Symposium 39: Interstellar Gas Dynamics, ed. Habing, p. 229.

Woltjer, L., 1972, Ann. Rev. Astron. Ap. 10, 129, "Supernova Remnants".

Wu, C.-C., Leventhal, M., Sarazin, C. L., and Gull, T. R., 1983, Ap. J. (Letters) 269, L5, "High-Velocity Iron Absorption Lines in Supernova Remnant 1006".

Zarnecki, J. C., and Culhane, J. L., 1977, MNRAS 178, 57P-61P, "Detection of OVIII Line Emission in the X-ray Spectrum of Puppis A".

Zarnecki, J. C., Culhane, J. L., Toor, A., Seward, F. D., and Charles, P. A., 1978, Ap. J. (Letters) 219, L17-L21, "The X-ray Spectrum and Structure of the Puppis A Supernova Remnant".

Zwicky, F., 1938, Phys. Rev. 54, 242, "On Neutron Stars".

1. Report No	2. Government Accession No	3 Recipient's Catalog No
NASA TM-86169		

4. Title and Subtitle	5 Report Date
X-Ray Spectra of Supernova Remnants	February 1985
	6 Performing Organization Code 661

7. Author(s)	8 Performing Organization Report No
Andrew E. Szymkowiak	M-37

9 Performing Organization Name and Address	10 Work Unit No
X-Ray Astronomy Group Laboratory for High Energy Astrophysics NASA/Goddard Space Flight Center Greenbelt, MD 20771	11 Contract or Grant No.
	13. Type of Report and Period Covered: Technical Memorandum
12 Sponsoring Agency Name and Address National Aeronautics and Space Administration Washington, DC 20546	14 Sponsoring Agency Code

15. Supplementary Notes

Andrew E. Szymkowiak: University of Maryland, College Park, Maryland; now at Goddard Space Flight Center, Greenbelt, Maryland.

Dissertation for Doctor of Philosophy, 1984, University of Maryland, Department of Physics and Astronomy.

16. Abstract

X-ray spectra were obtained from fields in three supernova remnants with the Solid State Spectrometer of the HEAO-2 satellite. These spectra, which contain lines from K-shell transitions of several abundant elements with atomic numbers between 10 and 22, were compared with various models, including some of spectra that would be produced by adiabatic phase remnants when the time-dependence of the ionization is considered.

17. Key Words (Selected by Author(s))	18 Distribution Statement
X-Ray Spectra Supernovae HEOS-2	Unclassified - Unlimited Star Category 89

19. Security Classif. (of this report)	20 Security Classif (of this page)	21. No of Pages	22 Price*
Unclassified	Unclassified	122	A06

*For sale by the National Technical Information Service, Springfield, Virginia 22151

NASA-Langley, 1985

End of Document